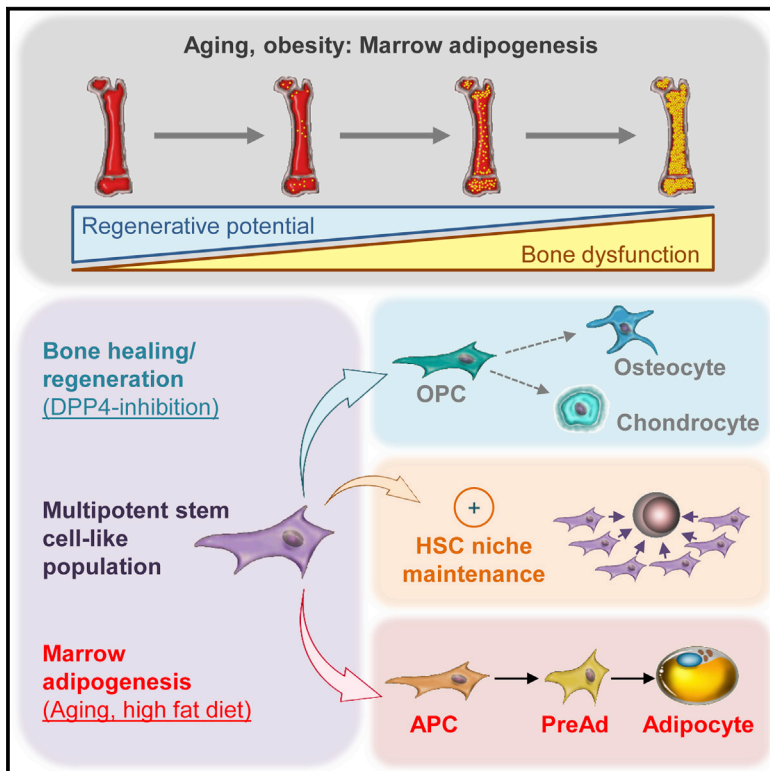# Adipocyte Accumulation in the Bone Marrow during Obesity and Aging Impairs Stem Cell-Based Hematopoietic and Bone Regeneration

Graphical Abstract

Highlights

- A stem cell-like population produces adipogenic and osteogenic lineages in bone

- Aging and high-fat diet specifically promote expansion of the adipogenic lineage

- Multipotent cells promote and adipogenic cells reduce hematopoietic reconstitution

- Adipogenic cells inhibit fracture repair, which is restored by DPP4 inactivation

Authors

Thomas H. Ambrosi,
Antonio Scialdone, Antonia Graja, ...,
Annette Schürmann, Luis R. Saraiva,
Tim J. Schulz

Correspondence

tim.schulz@dife.de

In Brief

Ambrosi, Schulz, and colleagues define a stem cell-like population that gives rise to osteogenic progeny and promotes hematopoietic reconstitution. Aging and high-fat diet reprogram the mesenchymal lineage to preferentially give rise to adipogenic cells that impair reconstitution and bone fracture healing. Bone tissue repair is fully restored by DPP4 inhibition.

CrossMark

CellPress

CellPress

Adipocyte Accumulation in the Bone Marrow during Obesity and Aging Impairs Stem Cell-Based Hematopoietic and Bone Regeneration

Thomas H. Ambrosi,[1] Antonio Scialdone,[2,3] Antonia Graja,[1] Sabrina Gohlke,[1] Anne-Marie Jank,[1] Carla Bocian,[1] Lena Woelk,[1] Hua Fan,[4] Darren W. Logan,[2,5] Annette Schürmann,[1,7] Luis R. Saraiva,[6] and Tim J. Schulz[1,7,8,*]

[1]German Institute of Human Nutrition Potsdam-Rehbrücke, 14558 Nuthetal, Germany
[2]Wellcome Trust Sanger Institute, Wellcome Genome Campus, Hinxton-Cambridge CB10 1SA, UK
[3]European Bioinformatics Institute (EMBL-EBI), European Molecular Biology Laboratory, Wellcome Genome Campus, Hinxton-Cambridge CB10 1SD, UK
[4]Charité Universitätsmedizin, Berlin 10117, Germany
[5]Monell Chemical Senses Center, Philadelphia, PA 19104, USA
[6]Sidra Medical and Research Center, Qatar Foundation, P.O. Box 26999, Doha, Qatar
[7]German Center for Diabetes Research (DZD), 85764 München-Neuherberg, Germany
[8]Lead Contact
*Correspondence: tim.schulz@dife.de
http://dx.doi.org/10.1016/j.stem.2017.02.009

SUMMARY

Aging and obesity induce ectopic adipocyte accumulation in bone marrow cavities. This process is thought to impair osteogenic and hematopoietic regeneration. Here we specify the cellular identities of the adipogenic and osteogenic lineages of the bone. While aging impairs the osteogenic lineage, high-fat diet feeding activates expansion of the adipogenic lineage, an effect that is significantly enhanced in aged animals. We further describe a mesenchymal sub-population with stem cell-like characteristics that gives rise to both lineages and, at the same time, acts as a principal component of the hematopoietic niche by promoting competitive repopulation following lethal irradiation. Conversely, bone-resident cells committed to the adipocytic lineage inhibit hematopoiesis and bone healing, potentially by producing excessive amounts of Dipeptidyl peptidase-4, a protease that is a target of diabetes therapies. These studies delineate the molecular identity of the bone-resident adipocytic lineage, and they establish its involvement in age-dependent dysfunction of bone and hematopoietic regeneration.

INTRODUCTION

The adipocyte-enriched yellow bone marrow develops during aging and obesity, and it may contribute to a dysfunction of the osteogenic and hematopoietic niches of long bones. According to recent data, increased marrow adipose tissue (MAT) in obese individuals is correlated with osteoporosis and increased fracture risk (Fazeli et al., 2013; Schwartz, 2015). Similarly, type II diabetes has been linked to reduced bone quality (Carnevale

et al., 2014). However, a causal relationship has not been fully established, as mice fed a high-fat diet also showed a rapid increase in MAT while bone parameters remained unaffected (Doucette et al., 2015). Nevertheless, marrow adipogenesis is associated with impaired hematopoiesis (Naveiras et al., 2009). Several seemingly opposing influences, such as aging and obesity but also caloric restriction and anorexia, irradiation therapy, thiazolidinediones, and glucocorticoids, promote the accumulation of MAT (Devlin and Rosen, 2015). Two types of MAT have been described: the constitutive MAT (cMAT), localized around the growth plates, and regulated MAT (rMAT), which accumulates later in life and in response to high-fat feeding (Scheller et al., 2015).

It has been proposed that MAT progenitors are radio-resistant, non-hematopoietic cells with a mesenchymal origin (Berry et al., 2015). Mesenchymal stromal cells (MSCs) are capable of giving rise to osteoblasts, chondroblasts, and adipocytes (Fridenshteĭn et al., 1968). Lineage tracing has linked the developmental origin of MSCs to Osterix1 (Osx1)-expressing cells in neonatal bone marrow (Mizoguchi et al., 2014) and to cells expressing Leptin receptor (LepR) in adult bone marrow (Zhou et al., 2014). Concomitantly, Leptin signaling regulates MAT formation and osteogenesis in adult mice (Yue et al., 2016). Subsets of bone marrow MSCs, such as C-X-C motif chemokine (CXCL)12-abundant reticular (CAR) cells, provide essential maintenance signals for the hematopoietic stem cell niche (Mendelson and Frenette, 2014; Morrison and Scadden, 2014).

The involvement of MAT in local osteogenic and immunomodulatory processes as well as systemic metabolism emphasizes the necessity to further investigate the adipogenic potential of bone marrow mesenchymal cells. Using a combination of flow cytometry and genetic lineage tracing, we delineate considerable cellular heterogeneities, and we identify distinct subsets of mesenchymal cells within the bone marrow cavity of the long bones in male mice. Specifically, we describe a multipotent population with stem cell-like properties residing within the perivascular niche that gives rise to unilaterally committed
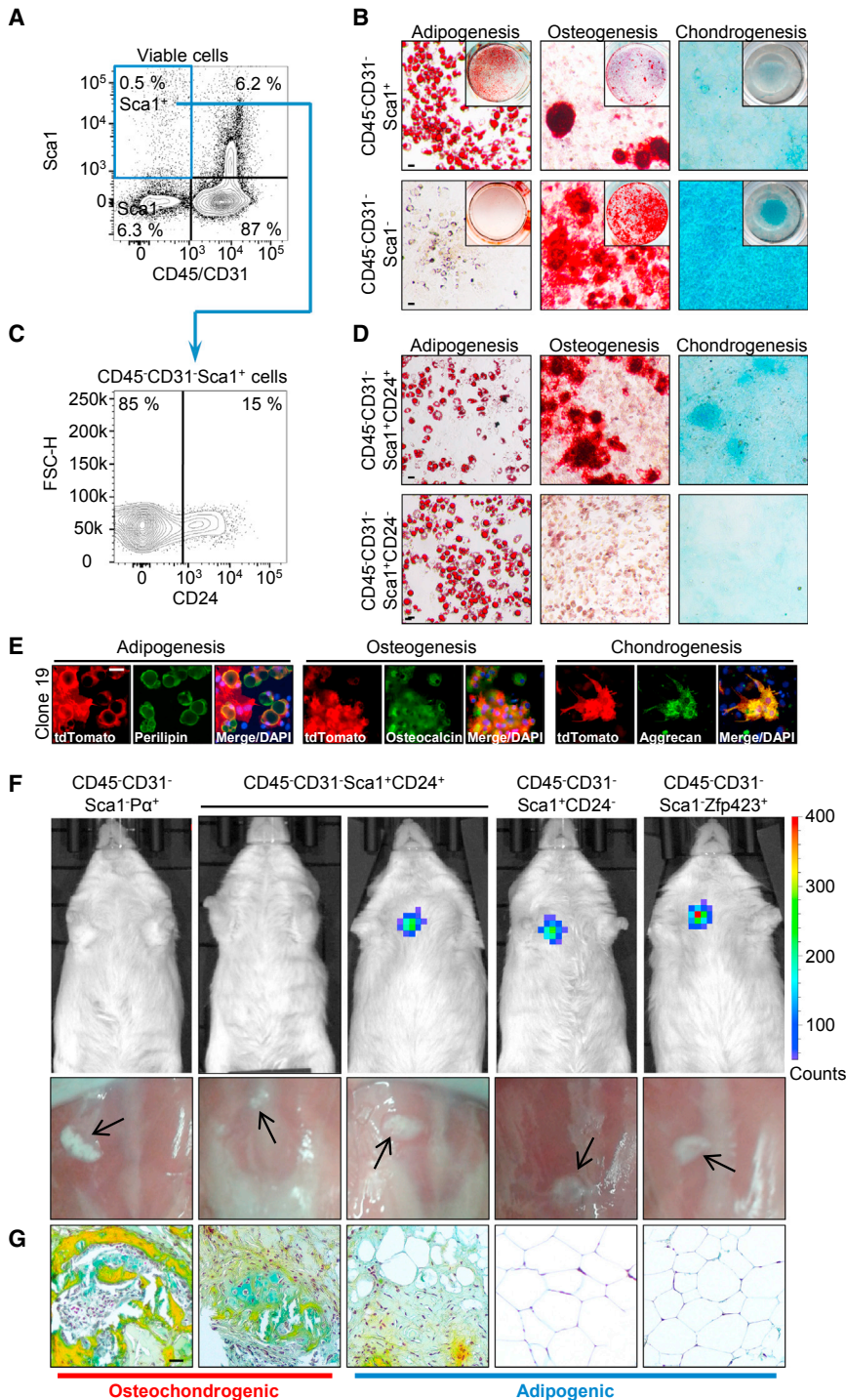
Figure 1. Bone Marrow-Resident Mesenchymal Cells Display Functional Heterogeneity

(A and B) Flow cytometric separation of CD31⁻CD45⁻ cells by Sca1 selection, followed by (B) Oil Red O (adipogenesis), Alizarin Red S (osteogenesis), and Alcian Blue (chondrogenesis) staining of Sca1⁺ and Sca1⁻ cells differentiated under the corresponding conditions.

(C and D) FACS analyses (as in A) of CD31⁻CD45⁻ Sca1⁺ cells separated by CD24 expression, and (D) subsequent differentiation of cells (as in B).

(E) Representative image of clonal analysis with feeder cells by co-staining of clone 19-derived tdTomato⁺ cells with Perilipin, Osteocalcin, or Aggrecan to show lineage-specific differentiation potential.

(F) In vivo luciferase imaging (top panels) and macroscopic identification (arrows; lower panels) of transplants 8 weeks after sternal subcutaneous (s.c.) injection of the indicated cell populations isolated from rep^AdiLuc mice.

(G) Microscopy of corresponding Movat-Pentachrome stains (yellow, mineralized structure; blue, cartilage; purple, nuclei. Scale bars, 30 μm. See also Figures S1–S3 and Tables S1–S4.

RESULTS

Identification of the Bone Adipocytic Lineage

To delineate the heterogeneous composition of the mesenchymal lineage of the bone, we used flow cytometry as reported in adipose tissues and bone (Morikawa et al., 2009a; Rodeheffer et al., 2008; Schulz et al., 2011; Tang et al., 2008). To this end, we isolated distinct populations of non-hematopoietic (Cluster of differentiation [CD]45⁻), non-endothelial (CD31⁻) cells that could be subdivided by expression of Stem cell antigen (Sca)1 into two subsets of culture-adherent fibroblasts also expressing the surface receptor platelet-derived growth factor-α (Pα; Figures 1A and S1A–S1C). During in vitro differentiation, CD45⁻ CD31⁻Sca1⁺ cells exhibited a highly adipogenic but limited osteochondrogenic potential. CD45⁻CD31⁻Sca1⁻ cells, in turn, were non-adipogenic but markedly osteochondrogenic (Figure 1B).

sub-populations of osteochondrogenic and adipogenic lineages under in vitro and in vivo conditions. Adipocytic cells significantly impair hematopoietic repopulation and bone fracture healing. This latter effect is mediated by secreted Dipeptidyl peptidase-4 (DPP4), an important target of anti-diabetes treatments (Lamers et al., 2011; Marguet et al., 2000). These findings altogether support the hypothesis of a deteriorative role of MAT in bone health and hematopoiesis.

Consistent with white adipose tissue (Berry and Rodeheffer, 2013; Rodeheffer et al., 2008), we isolated a population of unilaterally committed adipogenic progenitors that was CD45⁻CD31⁻ Sca1⁺CD24⁻ and a CD45⁻CD31⁻Sca1⁺CD24⁺ population that displayed tri-lineage differentiation potentials (Figures 1C and 1D). Colony-forming unit (CFU-F) potentials and in vitro recovery rates were highest in fibroblastic cells expressing Sca1 and/or Pα and were highest in the CD45⁻CD31⁻Sca1⁺Pa⁺CD24⁺

subset (Figures S1D and S1E). CFU-F potential was enriched in the osteogenic CD45−CD31−Sca1−Pα+ population but absent in CD45−CD31−Sca1−Pα− cells. Separation of the osteogenic CD45−CD31−Sca1−Pα+ population by CD24 expression was also possible, but these subsets showed identical differentiation capacities (Figures S1F and S1G). Similarly, the CD45−CD31− Pα−Sca1− cells were mostly CD24+ but were non-CFU-F (Figures S1D and S1H). Importantly, two separate clonal analyses of the tri-potent CD45−CD31−Sca1+CD24+ population revealed a marked homogeneity of a multipotent phenotype, where 64 of 68 (94%) and 45 of 54 (83%) clones were able to differentiate into all three lineages when cultivated in the presence or without supporting feeder cells, respectively (Figures 1E and S1I; Table S1). The somewhat lower homogeneity in the feeder-free assay could be due to technical differences, such as replicative senescence, but it could also mean that this population relies on exposure to trophic signals from the microenvironment to retain long-term multipotency.

The transcription factor zinc-finger protein (Zfp)423 labels adipogenic cells in white adipose tissue (WAT) (Gupta et al., 2012). Surprisingly, but consistent with the initial report using a Zfp423-driven EGFP reporter strain (Zfp423-EGFP), Zfp423-EGFP+ (Zfp423+) cells occurred as a small sub-population of <1% within the CD45−CD31−Sca1− population, while all adipogenic CD45−CD31−Sca1+ cells were GFP− (Figure S1J). This small subset of adipogenic cells was likely not initially detected due to a dilution effect within the strongly osteochondrogenic cell fraction (Figure 1B). In culture, CD45−CD31−Sca1−Zfp423+ cells maintained GFP expression before and after differentiation into adipocytes (Figure S1K). In contrast, all CD45−CD31−Sca1+ cells uniformly acquired GFP expression only during differentiation, a process that correlated with a concomitant loss of Sca1 expression (Figures S1K–S1N).

In Pα-EGFP reporter mice, multipotent cells and osteogenic progenitors were more abundant in the metaphysis compared to the diaphysis, whereas adipogenic progenitors were evenly distributed. Further analyses of Pα, Sca1, and CD24 expression localized osteogenic progenitors to the endosteum. The majority of multipotent and adipogenic progenitors cells resided in a non-endosteal localization within 40 μm of the bone surface, and it revealed a perivascular association of all non-endosteal Pα+ cells to blood vessels of <10 μm in diameter (Figures S2A–S2E). These findings suggest different micro-anatomical localizations of these functionally distinct cell populations and a preferential association of perivascular multipotent and adipogenic cells to L type vessels, while the distribution of endosteal osteogenic cells resembles more closely localizations of H type endothelium (Itkin et al., 2016; Kusumbe et al., 2014). Consistent with the preferential occurrence of adipocytes in the bone tips of young mice, Zfp423+ cells mainly localized to metaphyseal regions of the bone, and they labeled a subset of blood vessel-associated progenitors alongside all mature adipocytes of the marrow cavity (Figures S2F–S2H).

Together, these findings indicate the presence of at least four distinct cell populations in defined micro-anatomies within the bone: a tri-potent, perivascular population with stem cell-like characteristics (CD45−CD31−Sca1+CD24+), two functionally and anatomically distinct progenitor populations that are fate-committed toward either the osteochondrogenic (CD45−CD31−

Sca1−Pα+) or adipogenic (CD45−CD31−Sca1+CD24−) lineages, and a more mature CD45−CD31−Sca1−Zfp423+ adipocyte precursor stage. All four populations were present in different bone compartments (Table S2) and all CD45−CD31−Sca1+ cells were adipogenic (Figure S2I). No correlations between MAT occurrence and cell frequencies were evident, and we conclude that regulatory signals, such as leptin, may determine the progression into mature adipocytes. Since Sca1+ adipogenic progenitors are also more evenly distributed compared to mature Zfp423+ cells (Figures S2B and S2H), this implies that signals preventing adipogenic maturation could be differentially distributed within the bones of young mice.

To test in vivo differentiation potentials, we generated a triple-transgenic mouse strain carrying alleles of the Zfp423-EGFP reporter, Adiponectin (Adipoq)-Cre, and a luciferase reporter within the Rosa26 locus that is only expressed after Cre-mediated recombination, e.g., in mature adipocytes (rep^{AdiLuc}, Figure S2J), and we generated a second strain with constitutive red fluorescence (mTmG reporter allele) crossed to the Zfp423-EGFP reporter (rep^{tdTom}; Figure S2K). Fresh cells of all four populations isolated from rep^{AdiLuc} or rep^{tdTom} by fluorescence-activated cell sorting (FACS) (Figure S2L) were transplanted into the sternal region of B6/Albino mice. After 8 weeks, in vivo imaging of luciferase and Perilipin immunofluorescence (IF) showed that transplants of the CD45−CD31−Sca1+CD24− and CD45−CD31−Sca1−Zfp423+ adipogenic populations consistently gave rise to bona fide mature adipocytes, while in vitro osteogenic CD45−CD31−Sca1−Pα+ cells did not (Figures 1F, 1G, S3A, and S3B). Interestingly, CD45−CD31−Sca1+CD24+ cells gave rise to luciferase-positive and -negative transplants (Figure 1F). Movat-Pentachrome staining of luciferase-negative tissues of CD45−CD31−Sca1+CD24+ and CD45−CD31−Sca1− Pα+ cells revealed bone-like osteochondrogenic/mineralized structures but never adipocytes (Figures 1G and S3C). Consistent with this observation, intratibial injections of the four cell populations showed that only CD45−CD31−Sca1+CD24+, CD45−CD31−Sca1+CD24−, and CD45−CD31−Sca1−Zfp423+ cells, but never CD45−CD31−Sca1−Pα+, gave rise to Zfp423+ adipogenic cells in their endogenous microenvironment (Figure S3D). Moreover, only CD45−CD31−Sca1+CD24+ transplants were able to give rise to adipogenic CD45−CD31−Sca1+CD24− cells (Figure S3E). In summary, these findings reveal a multi-lineage potential of the CD45−CD31−Sca1+CD24+ cell population that can give rise to a lineage of fate-committed adipogenic progenitor cells (APCs: CD45−CD31−Sca1+CD24−) that, in turn, give rise to a more mature pre-adipocyte (preAd: CD45−CD31− Sca1−Zfp423+) and that, in parallel, could yield a population of unilaterally committed osteochondrogenic progenitor cells (OPCs: CD45−CD31−Sca1−Pα+), under in vitro and vivo conditions (Tables S3 and S4).

Osteo-Adipogenic Cell Populations Derive from a Mesenchymal, Non-endothelial, Non-hematopoietic Lineage

To determine the developmental lineages of these four cell populations, lineage tracing was performed using mouse strains expressing Cre-recombinase under the control of promoters to mark hematopoietic (Vav1), endothelial (Cdh5 and Tek/Tie2), or mesenchymal (Prx1 and Pα) cells, or mature adipocytes (Adipoq)

that were crossed to the mTmG-reporter mouse strain (Berry and Rodeheffer, 2013; Krueger et al., 2014). IF and flow cytometric analysis revealed a non-hematopoietic, non-endothelial, but mesenchymal lineage for the bone marrow-resident cells with purely adipogenic (APCs, adipocytes) or osteogenic (bone lining, osteocytes) potentials, which was also true for the CD45$^-$CD31$^-$Sca1$^+$CD24$^+$ stem cell-like population with tri-lineage potential (Figures 2A–2C).

As shown in previous reports on adipose tissues, CD45$^+$ hematopoietic cells were exclusively traced by Vav1-Cre, whereas CD31$^+$ cells did not trace to the expected Cdh5-Cre endothelial origin but rather to the Vav1-Cre hematopoietic driver (Figure 2D) (Berry and Rodeheffer, 2013). Unexpectedly, only ~50% of marrow adipocytes and CD45$^-$CD31$^-$Sca1$^+$ APCs were marked by the Pα-Cre driver (Figure 2), contradicting our data from the Pα-EGFP reporter and also from the FACS analyses (Figure S3F), but consistent with previous reports of incomplete recombination by this Cre strain (Krueger et al., 2014; Zhou et al., 2014). Lastly, comparing the developmental lineages of adipogenic progenitors in Prx1-Cre:mTmG mice revealed labeling of inguinal WAT (iWAT) and skeletal muscle-resident CD45$^-$CD31$^-$Sca1$^+$ cells that were comparable to bone, while brown adipose tissue (BAT) and epididymal WAT (eWAT) progenitors displayed almost no labeling (Figure S3G). Moreover, gene expression patterns of in-vitro-differentiated progenitors from bone resembled most closely those derived from iWAT, with similar adipogenic differentiation capacity and expression of general adipogenic genes Peroxisome proliferator-activated receptor-γ (Pparg) and CCAAT/enhancer-binding protein-α (Cebpa) and absent or low expression of BAT markers Uncoupling protein-1 (Ucp1) and Cell Death-Inducing DFFA-Like Effector A (Cidea) (Figures S3H–S3M), altogether indicating that the marrow adipocytic lineage is more closely related to white rather than brown adipocytes.

The Adipocytic Lineage Responds to Diet and Aging

We next examined gene expression in femora and tibiae from young (2 months) and old (25 months) mice. Consistent with previous reports (Devlin and Rosen, 2015), expression of adipogenic marker Pparg was increased in old bones. However, adipogenic potential of CD45$^-$CD31$^-$Sca1$^+$ progenitors isolated from old bones was unchanged. Conversely, osteogenic marker Osterix (Osx/Sp7) expression was significantly reduced, as was osteogenic capacity of CD45$^-$CD31$^-$Sca1$^-$ progenitors (Figures S4A–S4C). Next, mice of both ages were fed a high-fat diet for either 24 hr (1dHFD) or 10 days (10dHFD). Accumulation of MAT was more pronounced in old animals after 10dHFD, while loss of trabecular bone was observed in aged animals independent of diet (Figure 3A). FACS analysis of young bones revealed a significant induction of CD45$^-$CD31$^-$Sca1$^+$CD24$^+$ and APC frequencies after 1dHFD that were no longer apparent in 10dHFD mice, suggesting that the rapid induction of adipocytic progenitor proliferation is a mechanism of short-term adaptation to diet (Figures 3B and S4D). In mice aged 25 months, the same 1dHFD stimulus significantly increased the multipotent CD45$^-$CD31$^-$Sca1$^+$CD24$^+$ and APC populations by ~3- and 2-fold, respectively (Figure 3B).

BrdU incorporation was tested in young and 15-month-old Zfp423-EGFP mice, and it was significantly induced in multipotent CD45$^-$CD31$^-$Sca1$^+$CD24$^+$ cells and APCs, an effect that was more pronounced in APCs from old mice (Figure 3C). Conversely, the OPC population was not affected by 1dHFD (Figures 3B and S4E) and even showed a reduction in frequency and proliferation rates upon 10dHFD, an effect that was restricted to young animals (Figures S4D and S4F). In a cohort of aged, 15-month-old Zfp423-EGFP mice, cell frequencies of the Zfp423$^+$ preAds were significantly enhanced after 1dHFD, an effect that was significantly less pronounced in young animals (Figure 3D). Taken together, these findings on the bone-resident progenitor lineages could explain the enhanced accumulation of MAT observed during aging and in response to dietary cues.

Distinct Effects of Multipotent Cells and Committed Adipogenic Cells on Hematopoietic Reconstitution

Previous work has suggested a negative effect of MAT on hematopoiesis (Naveiras et al., 2009). To test this more directly, competitive repopulation assays after a dose of lethal irradiation (Luo et al., 2015) were performed after intratibial transplantation of the four cell populations (Figure 4A). As expected after irradiation (Scheller and Rosen, 2014), increased amounts of adipocytes were observed in all groups after 5 weeks, an effect that was more pronounced after transplantation of fate-committed APCs and Zfp423$^+$ preAds (Figure 4B). In full support of the sternal transplantation data, donor-derived (tdTomato$^+$) adipocytes were only observed when multipotent CD45$^-$CD31$^-$Sca1$^+$CD24$^+$ cells, APCs, or preAds, but not OPCs, were transplanted (Figure 4C). FACS analysis of bone marrows showed that donor-derived progenitors were retained 5 weeks after irradiation/transplantation, indicating long-term survival (Figure 4D, upper panels). Expression of Zfp423-driven EGFP was readily detectable in all marrows except after OPC transplants. All cells from the Zfp423$^+$ preAd transplants maintained GFP expression, indicating no reversion ability toward GFP$^-$ stages, whereas transplants of CD45$^-$CD31$^-$Sca1$^+$CD24$^+$ and APCs were only partially GFP$^+$, indicating that these cells maintained their original identity but also gave rise to maturing Zfp423$^+$ preAds (Figure 4D, middle panels). Consistent with our initial characterization, Zfp423$^+$ cells no longer expressed Sca1 or CD24 (Figure 4D, lower panels).

Tibiae that had received adipogenic transplants (APCs or preAds) 5 weeks prior to analysis showed significant reductions in cellularity but no change in overall bone marrow chimerism (Figures 4E and 4F). No differences in any of these parameters were observed in contralateral tibiae and regarding donor-derived myeloid and lymphoid cells, blood chimerism, or splenic hematopoietic progenitor cells, as these latter cells may also originate from other, non-injected bone sites (Figures 4E, 4F, and S5A–S5D). Importantly, frequencies of hematopoietic lineage (Lin)$^-$Sca1$^+$c-Kit$^+$ hematopoietic progenitor cells (LSK cells) and repopulation with donor-derived (CD45.1$^+$) CD34$^-$ long-term (LT)-LSK and CD34$^+$ short-term (ST)-LSK cells were significantly reduced after adipogenic transplants (Figures 4G–4I). A similar trend of impaired hematopoietic reconstitution was observed after transplantation of APCs in a separate long-term reconstitution experiment 16 weeks after irradiation, but it did not reach statistical significance (Figures S5E–S5G). Over the course of long-term reconstitution, no differences in blood
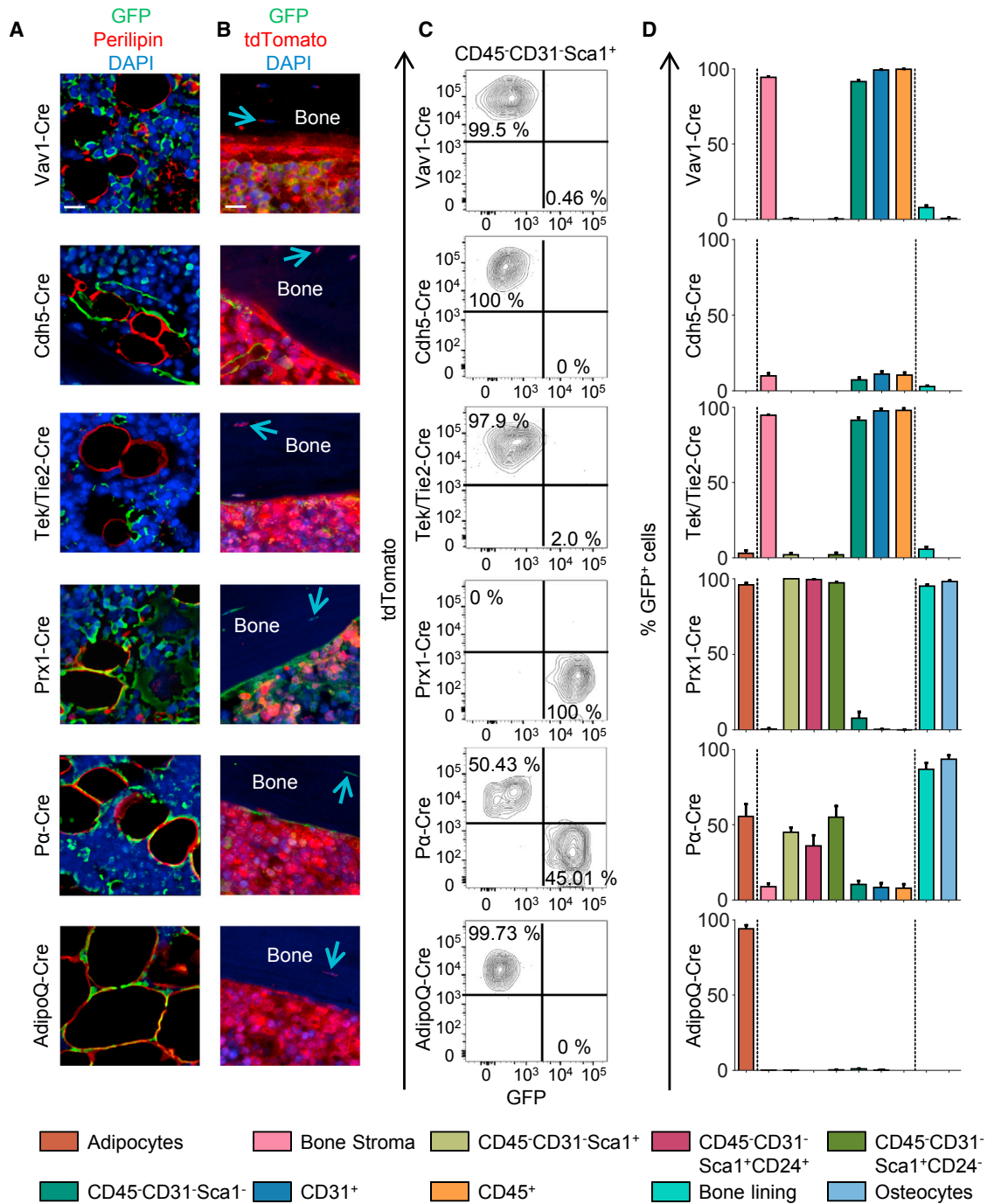
Figure 2. Lineage Tracing of MAT Reveals a Mesenchymal, Non-endothelial, Non-hematopoietic Lineage

(A) Representative merged IF images of bone-resident adipocytes from the indicated Cre-mTmG reporter mouse strains (green, EGFP; red, Perilipin; blue, DAPI).

(B) Reporter analysis of bone lining cells and cortical bone-resident osteocytes (blue arrows; green, GFP; red, tdTomato; blue, DAPI).

(C) FACS analysis of tdTomato$^+$ and GFP$^+$ cells in the CD45$^-$CD31$^-$Sca1$^+$ population (percentages represent average values).

(D) Quantification of GFP$^+$ bone-resident adipocytes, bone lining cells, and osteocytes by image quantification and flow cytometric analysis of bone stroma cells populations (n = 3–4 mice/genotype). Mean ± SEM. Scale bars, 10 μm.

See also Figure S3.

chimerism or blood lymphoid or blood myeloid cells were observed in animals transplanted with APCs (Figures S5H–S5J). FACS analysis revealed that transplanted cells were re-tained, and it confirmed that only CD45$^-$CD31$^-$Sca1$^+$CD24$^+$ and APCs gave rise to Zfp423$^+$ preAds, albeit at markedly lower frequencies (Figure S5K).
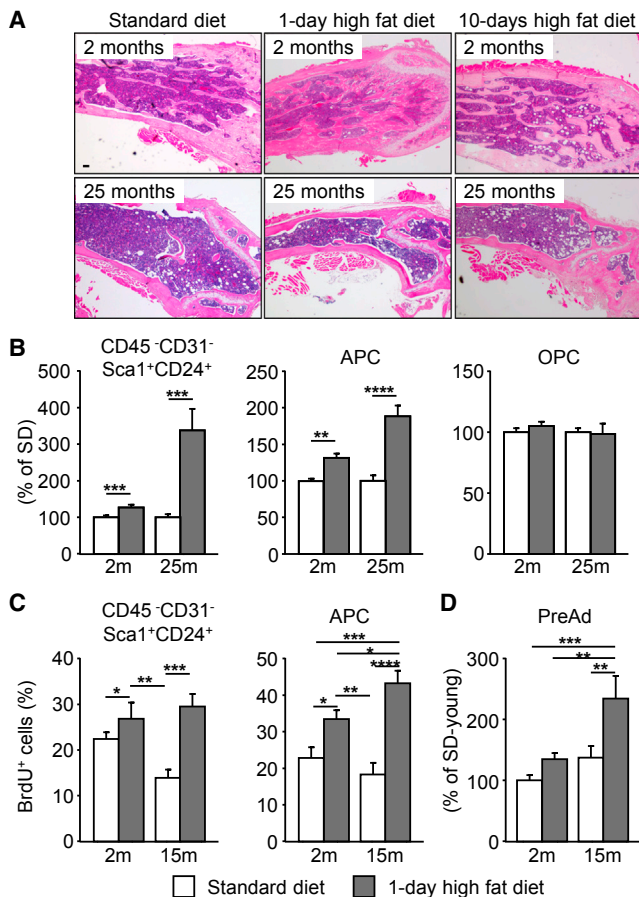
Figure 3. Aging and High-Fat Diet Stimulate Expansion of the Adipocytic Lineage

(A) H&E stains of femora from male mice aged 2 (young) or 25 months (old) maintained on standard diet (SD) or high-fat diet (HFD) for 24 hr (1dHFD) or 10 days (10dHFD).

(B) Relative quantifications of CD31⁻CD45⁻Sca1⁺CD24⁺, APC, and OPC populations in young and 25-month-old mice on SD (white bars) compared to 1dHFD (gray bars, applies to all panels) (n = 9).

(C) BrdU incorporation into CD31⁻CD45⁻Sca1⁺CD24⁺ and APCs from young and 15-month-old mice on SD or 1dHFD (n = 7–9).

(D) Quantification of GFP⁺ cells in 2-month- and 15-month-old male *Zfp423*-EGFP reporter mice on SD or 1dHFD (n = 6). Graphs show cumulative data from at least two independent experiments. Mean ± SEM; *p < 0.05, **p < 0.01, ***p < 0.001, and ****p < 0.0001. Scale bar, 100 μm.

See also Figure S4.

In contrast to adipogenic cells, transplantation of the multipotent CD45⁻CD31⁻Sca1⁺CD24⁺ population led to significantly increased repopulation with donor-derived LT-LSKs and ST-LSKs in tibiae at 5 and 16 weeks after irradiation, while overall bone marrow cellularity remained unchanged (Figures 4E–4I and S5E–S5G). Consistent with a potential involvement of this population in hematopoietic recovery, its relative frequency was transiently elevated after irradiation (Figure S5L). Taken together, these analyses further establish the developmental hierarchy among the four cell populations, and they reveal the potential of the CD45⁻CD31⁻Sca1⁺CD24⁺ multipotent cells to give rise to the adipocytic lineage under pro-adipogenic stimuli and at

the same time produce signals that support hematopoietic regeneration, whereas adipogenic cells significantly attenuate reconstitution.

The Adipocytic Lineage Inhibits Bone Regeneration

To determine the pathophysiological role of the adipocytic lineage during bone healing, all four populations isolated from rep^tdTom mice were transplanted into the vicinity of a stabilized tibia fracture and analyzed after 14 days (Figures 5A, upper panels, S6A, and S6B). The μCT quantification showed a significant decrease of total bone mineral density (BMD) at the fracture site following transplantation of adipogenic populations when compared to the no-cell control group (Figures 5A, middle panels, and 5B). Histomorphometric analysis of fracture/callus sites indicated reduced areas of mineralized tissue and increased amounts of cartilaginous tissues following transplantation of the adipogenic populations, e.g., APCs and preAds, compared to all other groups (Figures 5A, lower panels, and 5C–5E). Due to the lineage restrictions shown in the cell culture and sternal transplants, these observations likely indicate delayed healing and, thus, that the cartilaginous structures are entirely derived from the host in the adipogenic transplant groups. Aside from adopting an adipogenic fate after intratibial injection (Figure S3D), multipotent CD45⁻CD31⁻Sca1⁺CD24⁺ and the two adipogenic populations produced some fibrous tissue, whereas only multipotent CD45⁻CD31⁻Sca1⁺CD24⁺ and OPCs contributed to chondrogenic and osteogenic structures (Figures S6C–S6G). These observations indicate a negative regulatory role of adipocytic cells during fracture healing, further establishing the detrimental role of MAT in aged bone homeostasis.

DPP4 Released from MAT Inhibits Bone Healing

To identify potential negative regulators of regeneration processes, RNA sequencing (RNA-seq) was used to further characterize the molecular identity of all four populations (Figures S7A and S7B). Principal-component and hierarchical clustering analyses clearly supported the distinct nature of each population, providing a second line of evidence for the lineage restriction of adipogenic commitment of the closely related APC and preAd populations (Figures 6A–6C). Differential expression (DE) analysis produced several sets of known and potential new candidate genes to define each population (Figures 6D–6G; Table S5). For instance, canonical stem cell markers (e.g., *Nog*, *Il1rn*, and *Myc*) were enriched in the CD45⁻CD31⁻Sca1⁺CD24⁺ multipotent stem cell population (Figure 6D). Moreover, signals known to regulate hematopoietic stem cell (HSC) quiescence and maintenance (e.g., *Cxcl12*, *Kitl/Scf*, and *Vcam-1*), showed the highest expression in this population, along with the highest, but not exclusive, expression level of LepR that was also expressed in the other cells types. The OPC population expressed the classical osteogenic (e.g., *AlpI*, *Dmp1*, and *Col1α1/2*) and chondrogenic markers (e.g., *Acan*, *Col2α1*, and *Sox9*), as well as previously described skeletal stem cell markers (*Itga5* and *CD200*), at elevated levels (Figure 6E; Table S5) (Chan et al., 2015). The adipogenic populations expressed high levels of markers that have been linked to the adipocytic lineage (i.e., *Cd34*, *Ebf2*, and *Dpp4*) (Avogaro et al., 2014; Rodeheffer et al., 2008; Wang et al., 2014) or adipocyte differentiation (i.e., *Vim*, *Ppara*; Figures 6F and 6G) (Franke et al., 1987; Goto et al.,
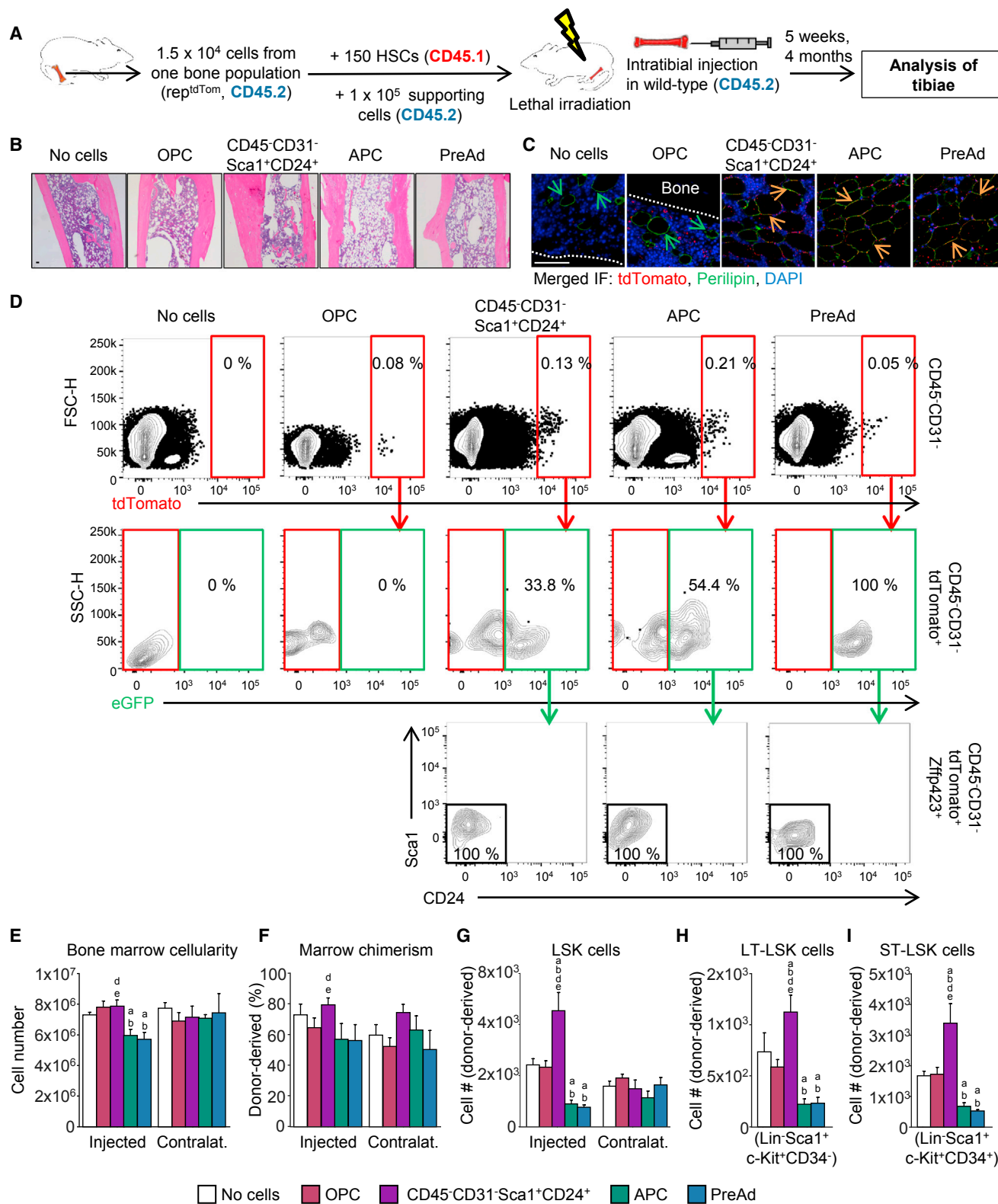
Figure 4. Distinct Roles of Progenitor Populations during Hematopoietic Recovery

(A) Schematic depiction of competitive hematopoietic repopulation assay.

(B and C) H&E stains of injected tibiae (B), and tdTomato (red) and Perilipin (green) (C) IF co-localization on adipocytes in injected tibiae (green arrow, host derived; orange arrow, donor derived). Scale bars, 50 μm.
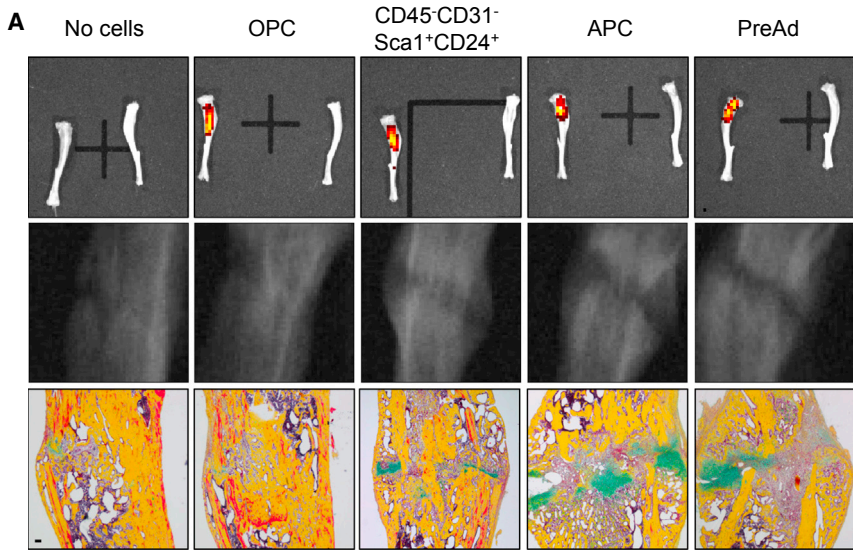
Figure 5. The Adipocytic Lineage Inhibits Bone Healing

(A) Red fluorescence in tibiae (top panels), μCT images (middle panels), and representative Movat-Pentachrome stains (lower panels; yellow, mineralized bone; red, new bone; blue, cartilage; purple, nuclei) of fracture calluses 14 days after fracture and intratibial injection of the indicated cell populations.

(B) Total bone mineral density (BMD) by μCT (n = 6).

(C–E) Histomorphometry of mineralized bone volume (BV) and non-mineralized callus (C) as fibrous tissue (FV) (D), and cartilage tissue (CV) volumes (E), all normalized to total callus volume (TV) (n = 8). Mean ± SEM; $p < 0.05$: a, versus no cells; b, versus OPC; and c, versus $CD31^-CD45^-Sca1^+CD24^+$. Scale bar, 100 μm.

See also Figure S6.
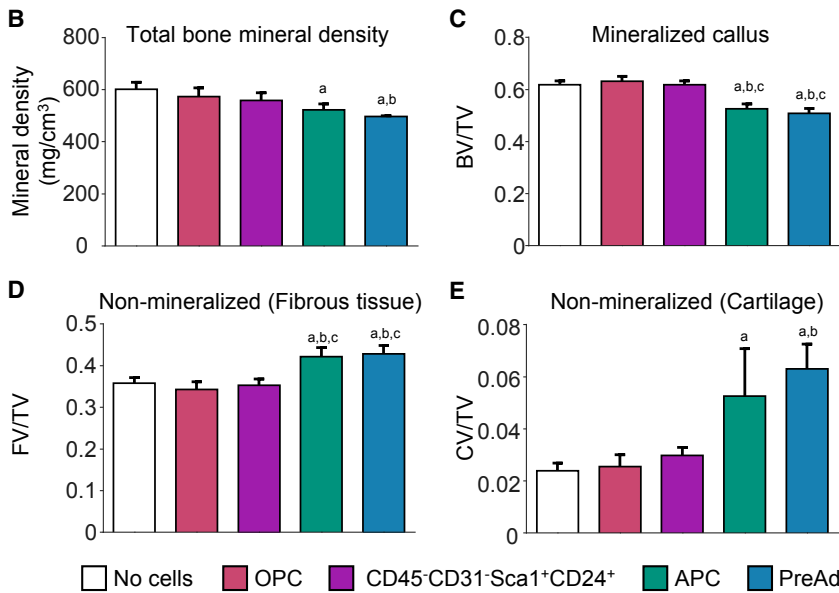
genic populations. Among the most significantly regulated secreted factors was the gene encoding for Dipeptidyl peptidase-4 (*Dpp4*), a protease shed from the plasma membrane that is an important target of clinical diabetes treatments (Figure 7A) (Avogaro et al., 2014; Marguet et al., 2000). Consistent with the RNA-seq data, CD26 (the membrane-bound form of DPP4) was enriched on the surface of adipogenic cell populations, and only $CD45^-CD31^-Sca1^+CD24^+$ and APCs, but not OPCs, released DPP4 into the medium after adipogenic differentiation (Figures S7C and S7D). Expression of *Dpp4* was increased in distal tibiae of old mice that contain most ectopic adipocytes, and explant cultures of old tibiae released greater amounts of DPP4 (Figures 7B and 7C). While treatment of $CD45^-CD31^-Sca1^+CD24^+$ and APCs with the DPP4 inhibitor sitagliptin

2011). As expected, expression of *Zfp423* was highest in Zfp423+ preAds (Figure 6F). Thus, our RNA-seq analysis confirmed the cellular characteristics of the four populations, and it establishes the $CD45^-CD31^-Sca1^+CD24^+$ multipotent stem cell population as a population expressing elevated levels of *Cxcl12* and *Lepr* that are important regulators of HSCs and osteogenesis (Greenbaum et al., 2013; Yue et al., 2016).

To identify signals that could mediate the negative effects of adipogenic cells on bone healing, we screened the dataset for secreted factors that were significantly enriched in the adipo-

had no effect on adipogenesis, it significantly enhanced osteogenic gene expression and mineralization of multipotent $CD45^-CD31^-Sca1^+CD24^+$ and OPCs during osteogenic differentiation (Figures 7D, 7E, S7E, and S7F). While no positive effect was found in untreated OPC transplants (Figure 5), the improved OPC function following sitagliptin may serve to promote bone healing. Exposure to recombinant DPP4 slightly impaired osteogenic, but did not alter adipogenic differentiation (Figures S7G–S7J). Treatment of mice with two DPP4 inhibitors, Diprotin A and sitagliptin, significantly accelerated tibia fracture healing

(D) Fate analyses of transplanted cells. $CD45^-CD31^-tdTomato^+$ cells (red squares, top row) were gated for expression of GFP (green squares, *Zfp423*-EGFP reporter; middle row). Zfp423+ cells were then assessed for expression of surface markers Sca1 and CD24 (bottom row).

(E–G) Bone marrow cellularity (E), marrow chimerism (F), and donor-derived (G) LSK cells in injected and contralateral tibiae 5 weeks after irradiation.

(H and I) Donor-derived LT-LSK (H) and donor-derived ST-LSK (I) hematopoietic stem cells in injected tibiae. Mean ± SEM (n = 7); $p < 0.05$: a, versus no cells; b, versus OPC; c, versus $CD31^-CD45^-Sca1^+CD24^+$; d, versus APC; and e, versus preAd.
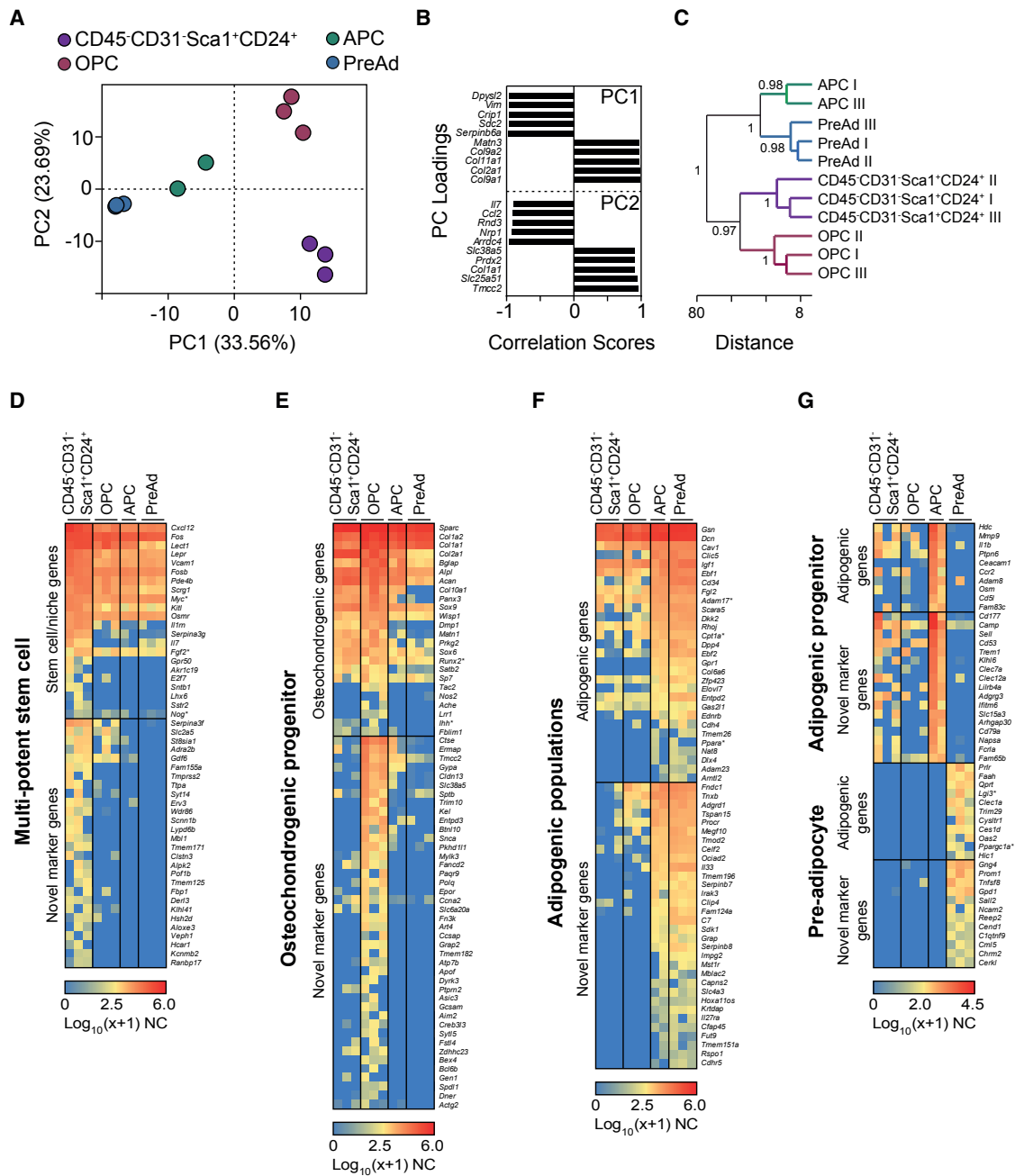
See also Figure S5.

Figure 6. RNA-Seq Defines the Cellular Identities of Bone-Resident Sub-populations

(A–C) The principal-component analysis (PCA; A), correlations scores (B) of the top ten genes driving PC1 and PC2 in (A), and hierarchical clustering analyses (C) of RNA-seq from all four cell populations.

(D–G) Heatmaps of selected differentially expressed (DE) genes, divided by candidates reported in the literature (known, asterisks indicate no significant DE between individual groups) and novel markers, enriched in CD31⁻CD45⁻Sca1⁺CD24⁺ (D), OPC (E), APCs and preAds combined (F), and APC or preAd (G) cell populations. See also Figure S7 and Table S5.

(Figures S7K and S7L), and intraperitoneal (i.p.) injections of sitagliptin for 9 days significantly increased the frequency of osteogenic progenitors while decreasing the frequency of APCs in non-fractured tibiae (Figure 7F). Administration of sitagliptin was sufficient to abolish the negative effects of transplanted adipogenic cells on bone healing while surprisingly promoting bone healing after OPC transplants (Figures 7G–7I). Lastly, transplan-

tation of *Dpp4*-deficient APCs similarly prevented the inhibitory effects of APCs on fracture healing (Figures 7J–7L).

DISCUSSION

Marrow adipogenesis is a highly regulated process that responds to a variety of endocrine signals, dietary cues, and
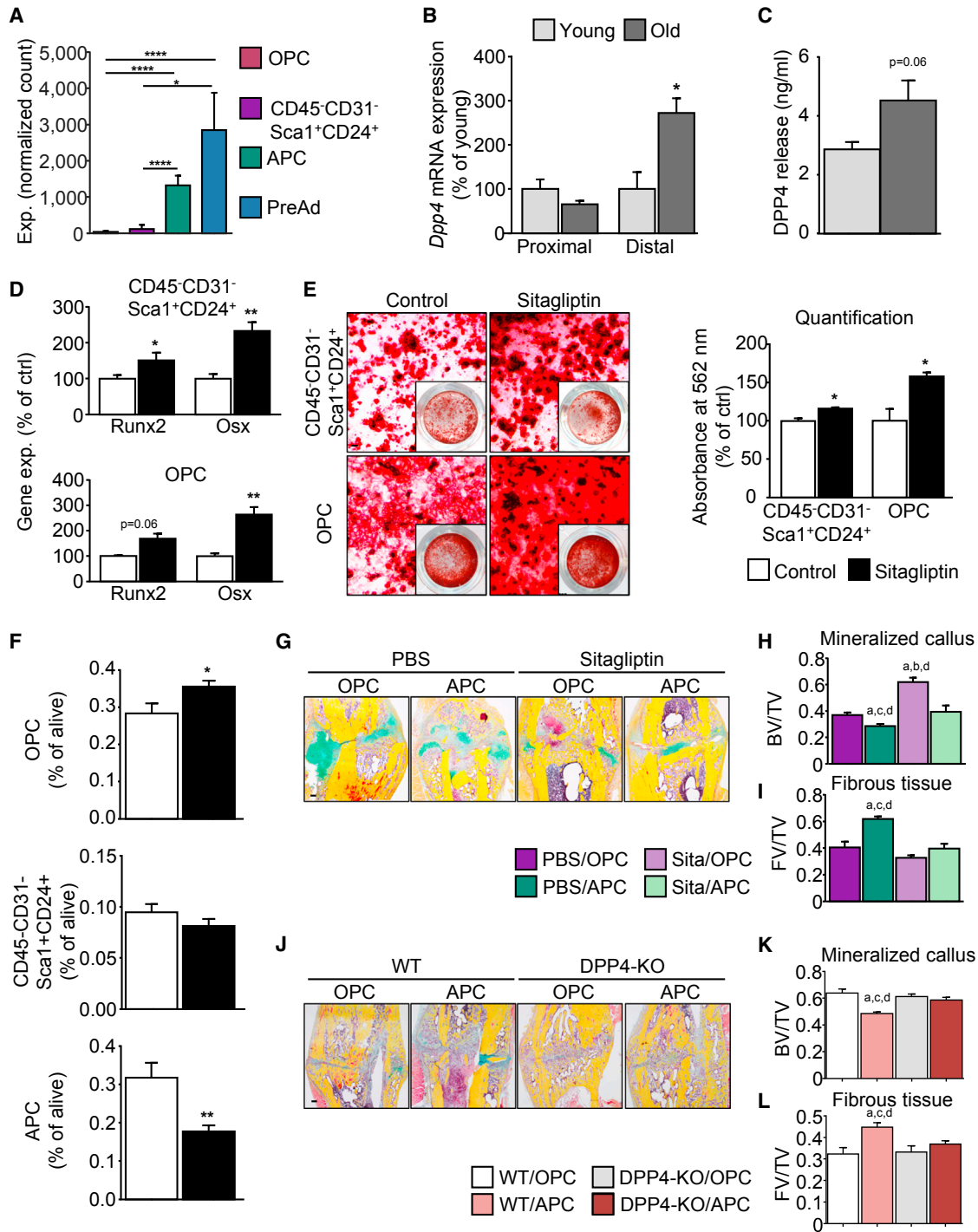
Figure 7. DPP4 Inhibition Reverses the Negative Effects of Adipogenic Cells on Bone Regeneration

(A) Gene expression intensities of *Dpp4* from RNA-seq analysis.

(B) *Dpp4*-mRNA levels in whole proximal and distal tibiae of young (2 months) and old (15 months) male mice (n = 5).

(C) DPP4 secretion by whole tibia explants from young and old mice (n = 4).

(D and E) The mRNA levels (D) of *Runx2* and *Osterix* (Osx/*Sp7*) and Alizarin Red S staining and quantification (E) of CD45⁻CD31⁻Sca1⁺CD24⁺ and OPCs either treated with PBS (control, white bars) or sitagliptin (100 μM, black bars) during osteogenic differentiation (n = 3). Scale bars, 30 μm.

(F) FACS analysis of OPC, CD45⁻CD31⁻Sca1⁺CD24⁺, and APC cell frequencies in tibiae from male mice either i.p. injected with PBS (white bars) or sitagliptin for 9 days (black bars; n = 9–10). Mean ± SEM; *p < 0.05, **p < 0.01, and ****p < 0.0001.

(G–I) Representative Movat-Pentachrome stains (G) of fracture calluses from control PBS-treated mice that received osteogenic (PBS/OPC) or adipogenic (PBS/APC) intratibial transplants and animals treated with sitagliptin for 1 week after fracture and receiving the same transplants of osteogenic (Sita/OPC)

(legend continued on next page)

pathologies (Scheller and Rosen, 2014), reflecting the necessity of a highly adaptive reservoir of stem/progenitor cells. Our study establishes a unidirectional developmental hierarchy of the bone marrow adipocytic lineage from a multipotent CD45−CD31−Sca1+CD24+ stem cell-like population toward distinct progenitor cell populations with unilaterally committed osteochondrogenic or adipogenic fates. Our results further suggest that adipogenic progenitors irreversibly mature toward a preAd stage: while APCs can maintain their identity they also give rise to Zfp423+ preAds that cannot revert to Sca1+Zfp423− progenitors. This unidirectional process enables the definition of two distinct maturation stages that subsequently differentiate into mature Zfp423+ marrow adipocytes. These findings are consistent with recent studies that have defined the heterogeneity of mesenchymal cell populations in WAT and BAT in some detail (Berry and Rodeheffer, 2013; Gupta et al., 2012; Rodeheffer et al., 2008; Schulz et al., 2011). The adipocytic as well as osteochondrogenic populations of the bone derive from a mesenchymal and non-hematopoietic, non-endothelial lineage. Previous work has also shown that neural crest-derived, Nestin+ cells are the likely developmental origin of the adult mesenchymal cells described here (Isern et al., 2014; Morikawa et al., 2009b; Nagoshi et al., 2008; Takashima et al., 2007).

Our data on developmental lineages, differentiation capacity, and adipocyte phenotype suggest that marrow-resident adipocyte progenitors more closely resemble white, rather than brown, adipogenic cells. This is consistent with previous reports, but it does not rule out specific differences in endocrine function between WAT and MAT (Scheller and Rosen, 2014). However, our RNA-seq analysis shows that several genes enriched in bone-resident preAds are also expressed in committed brown pre-adipocytes (e.g., *Ebf2*, *Entpd2*, *Fam129a*, and Acy3) (Wang et al., 2014), which would support at least some potential similarities to the BAT lineage (Krings et al., 2012).

A high-fat diet rapidly increases expansion of the adipogenic, but not the osteochondrogenic lineage. This induction is more pronounced in aged bone marrow. Whether aging also affects expansive capacities of subsets of adipose tissue-resident progenitors remains to be determined, but our data clearly suggest that this process may be involved in the pathogenic processes related to MAT accumulation. This observation is supported by a report on leptin-mediated regulation of diet-induced adipogenesis in the bone marrow (Yue et al., 2016). Of note, decreased numbers of OPCs after high-fat diet feeding were only observed in young animals, which could be due to leptin resistance as observed in aged animals (Gabriely et al., 2002) but which would also suggest that expansion of adipogenic cells may not be exclusively leptin dependent.

Sca1+ cells, e.g., the multipotent CD45−CD31−Sca1+CD24+ population, as well as APCs, associate to L type vessels that are known to host HSCs (Sivaraj and Adams, 2016) and occur in the vicinity of the endosteum and could, thereby, readily affect the hematopoietic niches or contribute to osteogenic processes. Interestingly, a multipotent differentiation potential of at least partially overlapping populations of bone-resident populations, such as PαS (Sca1+Pα+) cells, cells expressing LepR, or Nestin-expressing stromal cells, has been described before (Méndez-Ferrer et al., 2010; Morikawa et al., 2009a; Yue et al., 2016; Zhou et al., 2014), but these populations overlap at least partially with several of the populations described here. For instance, almost all LepR+ cells are Pα+ and contain all CD45−CD31−Sca1+ cells (Zhou et al., 2014). Our clonal analysis of CD45−CD31−Sca1+CD24+ cells identified this population as a highly homogeneous pool of multipotent cells, indicating additional enrichment in this stem cell-like sub-population. In support of this observation, clonal analysis of PαS or LepR+ cells showed multipotency only in a smaller subset of clones that may have derived from sub-populations expressing CD24 (Morikawa et al., 2009a; Zhou et al., 2014). Importantly, the multipotent stem cell-like population also promotes hematopoietic repopulation and is enriched for cells expressing the hematopoiesis maintenance cytokine CXCL12 (Greenbaum et al., 2013; Zhou et al., 2014). In comparison to the other three cell types defined in our study, we find that CD45−CD31−Sca1+CD24+ multipotent cells also express the highest levels of *Lepr* and other pro-hematopoietic signals, such as *Kitl/Scf* and *Vcam1*, and, thus, could represent a further purification step of a mesenchymal stem cell that supports hematopoiesis (Ding et al., 2012; Lewandowski et al., 2010). In summary, while we cannot exclude that several independent adipogenic and osteogenic lineages exist in bone, our study strongly suggests that the CD45−CD31−Sca1+CD24+ cell type, the skeletal equivalent of previously described adipocyte stem cells in WAT (Rodeheffer et al., 2008), can give rise to populations unilaterally committed to either lineage and provides maintenance signals essential for the hematopoietic niche.

Consistent with previous reports (Chan et al., 2015; Steenhuis et al., 2008), we describe a committed OPC population that may at least partially arise from the CD45−CD31−Sca1+CD24+ multipotent stem cells. Comparison of expression signatures suggests these correspond to previously described skeletal stem cells (Chan et al., 2015), which have been proposed to be one of two distinct skeletogenic stem cell populations contributing to post-natal development of bone (Worthley et al., 2015). In our study, *Grem1* mRNA was detected in all populations but was highest in the multipotent cells. While Worthley et al. (2015) clearly showed that Grem1+ cells are mostly CD45−CD31−Sca1− skeletal stem cells, a small subset of Grem1+ cells was also Sca1+ and could thus also mark the multipotent stem cell-like population we describe here. Further work is required to determine the extent to which CD45−CD31−Sca1+CD24+ cells contribute to the osteogenic lineages in embryonic and adult stages.

Ectopic adipocyte accumulation in the bone marrow cavity is believed to contribute to age-related impairment of bone

---

or adipogenic (Sita/APC) cells. Fracture callus total volumes (TVs) were analyzed for mineralized callus volume (H, BV/TV) and fibrous tissue volumes (I, FV/TV) (n = 5–7).

(J–L) Representative Movat-Pentachrome stains and histomorphometric analyses (as in G–I) of fracture calluses 14 days after injury from mice that received osteogenic (OPC) or adipogenic (APC) intratibial transplants from either DPP4-KO or wild-type (WT) animals (n = 9). Mean ± SEM; p < 0.05: a, versus PBS or WT/OPC; b, versus PBS or WT/APC; c, versus sitagliptin or DPP4-KO/OPC; and d, versus sitagliptin or DPP4-KO/APC. Scale bars, 100 μm.

See also Figure S7 and Table S6.

regeneration and hematopoiesis (Carnevale et al., 2014; Fazeli et al., 2013; Le et al., 2016; Naveiras et al., 2009; Schwartz, 2015). An increased risk for fractures and complications, such as non-unions, is associated with aging- and obesity-induced MAT accumulation (Nuttall and Gimble, 2004). Bone healing is tightly regulated with an initial inflammatory phase, followed by cartilaginous callus formation, the deposition of a fibrous matrix, and subsequent mineralization through osteogenic cells (Einhorn and Gerstenfeld, 2015). We here identify the cellular basis for the pro-adipogenic shift observed during high-fat diet feeding and aging. Cells committed to the adipogenic lineage not only inhibited bone healing but also acute hematopoietic reconstitution. The limited negative effect of the adipocytic lineage during long-term hematopoietic recovery further suggests that the lack of a pro-adipogenic stimulus is beneficial to bone homeostasis. Follow-up studies will have to determine whether these effects are also true for distinct processes, such as bone remodeling as opposed to bone healing, and subtypes of healthy and pathological MAT (Cawthorn et al., 2014; Scheller et al., 2015) and whether sex-specific differences occur as only male mice were analyzed in this study. A potential mediator of such detrimental effects on bone homeostasis is DPP4, as it was recently shown to impair hematopoietic recovery and bone health (Broxmeyer et al., 2012; Kim and Cho, 2016; Monami et al., 2011). Our results provide mechanistic insights into the beneficial effects of DPP4 inhibitors during bone regeneration by targeting the adipocytic lineage, and they potentially link MAT as a source of DPP4 to the pathophysiology of systemic insulin resistance. In summary, we here delineate the ontology of MAT and the adipocytic lineage, which exerts negative effects on bone healing and hematopoiesis. These findings suggest that MAT accumulation causes the age-related dysfunction of the bone marrow niches and can be implicated in multiple pathological processes that interfere with appropriate maintenance of bone tissue repair and the hematopoietic system.

STAR★METHODS

Detailed methods are provided in the online version of this paper and include the following:

REFERENCES

Avogaro, A., de Kreutzenberg, S., and Fadini, G. (2014). Dipeptidyl-peptidase 4 inhibition: linking metabolic control to cardiovascular protection. Curr. Pharm. Des. 20, 2387–2394.

Berry, R., and Rodeheffer, M.S. (2013). Characterization of the adipocyte cellular lineage in vivo. Nat. Cell Biol. 15, 302–308.

Berry, R., Rodeheffer, M.S., Rosen, C.J., and Horowitz, M.C. (2015). Adipose Tissue Residing Progenitors (Adipocyte Lineage Progenitors and Adipose Derived Stem Cells (ADSC). Curr. Mol. Biol. Rep. 1, 101–109.

Broxmeyer, H.E., Hoggatt, J., O'Leary, H.A., Mantel, C., Chitteti, B.R., Cooper, S., Messina-Graham, S., Hangoc, G., Farag, S., Rohrabaugh, S.L., et al. (2012). Dipeptidylpeptidase 4 negatively regulates colony-stimulating factor activity and stress hematopoiesis. Nat. Med. 18, 1786–1796.

Carnevale, V., Romagnoli, E., D'Erasmo, L., and D'Erasmo, E. (2014). Bone damage in type 2 diabetes mellitus. Nutr. Metab. Cardiovasc. Dis. 24, 1151–1157.

Cawthorn, W.P., Scheller, E.L., Learman, B.S., Parlee, S.D., Simon, B.R., Mori, H., Ning, X., Bree, A.J., Schell, B., Broome, D.T., et al. (2014). Bone marrow adipose tissue is an endocrine organ that contributes to increased circulating adiponectin during caloric restriction. Cell Metab. 20, 368–375.

Chan, C.K., Seo, E.Y., Chen, J.Y., Lo, D., McArdle, A., Sinha, R., Tevlin, R., Seita, J., Vincent-Tompkins, J., Wearda, T., et al. (2015). Identification and specification of the mouse skeletal stem cell. Cell 160, 285–298.

Devlin, M.J., and Rosen, C.J. (2015). The bone-fat interface: basic and clinical implications of marrow adiposity. Lancet Diabetes Endocrinol. 3, 141–147.

Ding, L., Saunders, T.L., Enikolopov, G., and Morrison, S.J. (2012). Endothelial and perivascular cells maintain haematopoietic stem cells. Nature 481, 457–462.

Doucette, C.R., Horowitz, M.C., Berry, R., MacDougald, O.A., Anunciado-Koza, R., Koza, R.A., and Rosen, C.J. (2015). A High Fat Diet Increases Bone Marrow Adipose Tissue (MAT) But Does Not Alter Trabecular or Cortical Bone Mass in C57BL/6J Mice. J. Cell. Physiol. 230, 2032–2037.

Einhorn, T.A., and Gerstenfeld, L.C. (2015). Fracture healing: mechanisms and interventions. Nat. Rev. Rheumatol. 11, 45–54.

Fazeli, P.K., Horowitz, M.C., MacDougald, O.A., Scheller, E.L., Rodeheffer, M.S., Rosen, C.J., and Klibanski, A. (2013). Marrow fat and bone–new perspectives. J. Clin. Endocrinol. Metab. 98, 935–945.

Franke, W.W., Hergt, M., and Grund, C. (1987). Rearrangement of the vimentin cytoskeleton during adipose conversion: formation of an intermediate filament cage around lipid globules. Cell 49, 131–141.

Fridenshteĭn, A.Ia., Petrakova, K.V., Kuralesova, A.I., and Frolova, G.I. (1968). [Precursor cells for osteogenic and hemopoietic tissues. Analysis of heterotopic transplants of bone marrow]. Tsitologiia 10, 557–567.

Gabriely, I., Ma, X.H., Yang, X.M., Rossetti, L., and Barzilai, N. (2002). Leptin resistance during aging is independent of fat mass. Diabetes 51, 1016–1021.

Goto, T., Lee, J.Y., Teraminami, A., Kim, Y.I., Hirai, S., Uemura, T., Inoue, H., Takahashi, N., and Kawada, T. (2011). Activation of peroxisome proliferator-activated receptor-alpha stimulates both differentiation and fatty acid oxidation in adipocytes. J. Lipid Res. 52, 873–884.

Greenbaum, A., Hsu, Y.M., Day, R.B., Schuettpelz, L.G., Christopher, M.J., Borgerding, J.N., Nagasawa, T., and Link, D.C. (2013). CXCL12 in early mesenchymal progenitors is required for haematopoietic stem-cell maintenance. Nature 495, 227–230.

Gupta, R.K., Mepani, R.J., Kleiner, S., Lo, J.C., Khandekar, M.J., Cohen, P., Frontini, A., Bhowmick, D.C., Ye, L., Cinti, S., and Spiegelman, B.M. (2012). Zfp423 expression identifies committed preadipocytes and localizes to adipose endothelial and perivascular cells. Cell Metab. 15, 230–239.

Isern, J., García-García, A., Martín, A.M., Arranz, L., Martín-Pérez, D., Torroja, C., Sánchez-Cabo, F., and Méndez-Ferrer, S. (2014). The neural crest is a source of mesenchymal stem cells with specialized hematopoietic stem cell niche function. eLife 3, e03696.

Itkin, T., Gur-Cohen, S., Spencer, J.A., Schajnovitz, A., Ramasamy, S.K., Kusumbe, A.P., Ledergor, G., Jung, Y., Milo, I., Poulos, M.G., et al. (2016). Distinct bone marrow blood vessels differentially regulate haematopoiesis. Nature 532, 323–328.

Kim, S.W., and Cho, E.H. (2016). High Levels of Serum DPP-4 Activity Are Associated with Low Bone Mineral Density in Obese Postmenopausal Women. Endocrinol. Metab. (Seoul) 31, 93–99.

Krings, A., Rahman, S., Huang, S., Lu, Y., Czernik, P.J., and Lecka-Czernik, B. (2012). Bone marrow fat has brown adipose tissue characteristics, which are attenuated with aging and diabetes. Bone 50, 546–552.

Krueger, K.C., Costa, M.J., Du, H., and Feldman, B.J. (2014). Characterization of Cre recombinase activity for in vivo targeting of adipocyte precursor cells. Stem Cell Reports 3, 1147–1158.

Kusumbe, A.P., Ramasamy, S.K., and Adams, R.H. (2014). Coupling of angiogenesis and osteogenesis by a specific vessel subtype in bone. Nature 507, 323–328.

Lamers, D., Famulla, S., Wronkowitz, N., Hartwig, S., Lehr, S., Ouwens, D.M., Eckardt, K., Kaufman, J.M., Ryden, M., Müller, S., et al. (2011). Dipeptidyl peptidase 4 is a novel adipokine potentially linking obesity to the metabolic syndrome. Diabetes 60, 1917–1925.

Le, Y., Fraineau, S., Chandran, P., Sabloff, M., Brand, M., Lavoie, J.R., Gagne, R., Rosu-Myles, M., Yauk, C.L., Richardson, R.B., and Allan, D.S. (2016). Adipogenic Mesenchymal Stromal Cells from Bone Marrow and Their Hematopoietic Supportive Role: Towards Understanding the Permissive Marrow Microenvironment in Acute Myeloid Leukemia. Stem Cell Rev. 12, 235–244.

Lewandowski, D., Barroca, V., Ducongé, F., Bayer, J., Van Nhieu, J.T., Pestourie, C., Fouchet, P., Tavitian, B., and Roméo, P.H. (2010). In vivo cellular imaging pinpoints the role of reactive oxygen species in the early steps of adult hematopoietic reconstitution. Blood 115, 443–452.

Luo, Y., Chen, G.L., Hannemann, N., Ipseiz, N., Krönke, G., Bäuerle, T., Munos, L., Wirtz, S., Schett, G., and Bozec, A. (2015). Microbiota from Obese Mice Regulate Hematopoietic Stem Cell Differentiation by Altering the Bone Niche. Cell Metab. 22, 886–894.

Marguet, D., Baggio, L., Kobayashi, T., Bernard, A.M., Pierres, M., Nielsen, P.F., Ribel, U., Watanabe, T., Drucker, D.J., and Wagtmann, N. (2000). Enhanced insulin secretion and improved glucose tolerance in mice lacking CD26. Proc. Natl. Acad. Sci. USA 97, 6874–6879.

Mendelson, A., and Frenette, P.S. (2014). Hematopoietic stem cell niche maintenance during homeostasis and regeneration. Nat. Med. 20, 833–846.

Méndez-Ferrer, S., Michurina, T.V., Ferraro, F., Mazloom, A.R., Macarthur, B.D., Lira, S.A., Scadden, D.T., Ma'ayan, A., Enikolopov, G.N., and Frenette, P.S. (2010). Mesenchymal and haematopoietic stem cells form a unique bone marrow niche. Nature 466, 829–834.

Mizoguchi, T., Pinho, S., Ahmed, J., Kunisaki, Y., Hanoun, M., Mendelson, A., Ono, N., Kronenberg, H.M., and Frenette, P.S. (2014). Osterix marks distinct waves of primitive and definitive stromal progenitors during bone marrow development. Dev. Cell 29, 340–349.

Monami, M., Dicembrini, I., Antenore, A., and Mannucci, E. (2011). Dipeptidyl peptidase-4 inhibitors and bone fractures: a meta-analysis of randomized clinical trials. Diabetes Care 34, 2474–2476.

Morikawa, S., Mabuchi, Y., Kubota, Y., Nagai, Y., Niibe, K., Hiratsu, E., Suzuki, S., Miyauchi-Hara, C., Nagoshi, N., Sunabori, T., et al. (2009a). Prospective identification, isolation, and systemic transplantation of multipotent mesenchymal stem cells in murine bone marrow. J. Exp. Med. 206, 2483–2496.

Morikawa, S., Mabuchi, Y., Niibe, K., Suzuki, S., Nagoshi, N., Sunabori, T., Shimmura, S., Nagai, Y., Nakagawa, T., Okano, H., and Matsuzaki, Y. (2009b). Development of mesenchymal stem cells partially originate from the neural crest. Biochem. Biophys. Res. Commun. 379, 1114–1119.

Morrison, S.J., and Scadden, D.T. (2014). The bone marrow niche for haematopoietic stem cells. Nature 505, 327–334.

Nagoshi, N., Shibata, S., Kubota, Y., Nakamura, M., Nagai, Y., Satoh, E., Morikawa, S., Okada, Y., Mabuchi, Y., Katoh, H., et al. (2008). Ontogeny and multipotency of neural crest-derived stem cells in mouse bone marrow, dorsal root ganglia, and whisker pad. Cell Stem Cell 2, 392–403.

Naveiras, O., Nardi, V., Wenzel, P.L., Hauschka, P.V., Fahey, F., and Daley, G.Q. (2009). Bone-marrow adipocytes as negative regulators of the haematopoietic microenvironment. Nature 460, 259–263.

Nuttall, M.E., and Gimble, J.M. (2004). Controlling the balance between osteoblastogenesis and adipogenesis and the consequent therapeutic implications. Curr. Opin. Pharmacol. 4, 290–294.

Rodeheffer, M.S., Birsoy, K., and Friedman, J.M. (2008). Identification of white adipocyte progenitor cells in vivo. Cell 135, 240–249.

Scheller, E.L., and Rosen, C.J. (2014). What's the matter with MAT? Marrow adipose tissue, metabolism, and skeletal health. Ann. N Y Acad. Sci. 1311, 14–30.

Scheller, E.L., Doucette, C.R., Learman, B.S., Cawthorn, W.P., Khandaker, S., Schell, B., Wu, B., Ding, S.Y., Bredella, M.A., Fazeli, P.K., et al. (2015). Region-specific variation in the properties of skeletal adipocytes reveals regulated and constitutive marrow adipose tissues. Nat. Commun. 6, 7808.

Schulz, T.J., Huang, T.L., Tran, T.T., Zhang, H., Townsend, K.L., Shadrach, J.L., Cerletti, M., McDougall, L.E., Giorgadze, N., Tchkonia, T., et al. (2011). Identification of inducible brown adipocyte progenitors residing in skeletal muscle and white fat. Proc. Natl. Acad. Sci. USA 108, 143–148.

Schwartz, A.V. (2015). Marrow fat and bone: review of clinical findings. Front. Endocrinol. (Lausanne) 6, 40.

Sivaraj, K.K., and Adams, R.H. (2016). Blood vessel formation and function in bone. Development 143, 2706–2715.

Steenhuis, P., Pettway, G.J., and Ignelzi, M.A., Jr. (2008). Cell surface expression of stem cell antigen-1 (Sca-1) distinguishes osteo-, chondro-, and adipoprogenitors in fetal mouse calvaria. Calcif. Tissue Int. 82, 44–56.

Takashima, Y., Era, T., Nakao, K., Kondo, S., Kasuga, M., Smith, A.G., and Nishikawa, S. (2007). Neuroepithelial cells supply an initial transient wave of MSC differentiation. Cell 129, 1377–1388.

Tang, W., Zeve, D., Suh, J.M., Bosnakovski, D., Kyba, M., Hammer, R.E., Tallquist, M.D., and Graff, J.M. (2008). White fat progenitor cells reside in the adipose vasculature. Science 322, 583–586.

Wang, W., Kissig, M., Rajakumari, S., Huang, L., Lim, H.W., Won, K.J., and Seale, P. (2014). Ebf2 is a selective marker of brown and beige adipogenic precursor cells. Proc. Natl. Acad. Sci. USA 111, 14466–14471.

Worthley, D.L., Churchill, M., Compton, J.T., Tailor, Y., Rao, M., Si, Y., Levin, D., Schwartz, M.G., Uygur, A., Hayakawa, Y., et al. (2015). Gremlin 1 identifies a skeletal stem cell with bone, cartilage, and reticular stromal potential. Cell *160*, 269–284.

Yue, R., Zhou, B.O., Shimada, I.S., Zhao, Z., and Morrison, S.J. (2016). Leptin Receptor Promotes Adipogenesis and Reduces Osteogenesis by Regulating Mesenchymal Stromal Cells in Adult Bone Marrow. Cell Stem Cell *18*, 782–796.

Zhou, B.O., Yue, R., Murphy, M.M., Peyer, J.G., and Morrison, S.J. (2014). Leptin-receptor-expressing mesenchymal stromal cells represent the main source of bone formed by adult bone marrow. Cell Stem Cell *15*, 154–168.

STAR★METHODS

KEY RESOURCES TABLE

REAGENT or RESOURCE	SOURCE	IDENTIFIER
Antibodies		
Anti-Mouse Ly-6A/E (Sca-1) APC (Clone: D7)	eBioscience	Cat#: 17-5981
Anti-Mouse Ly-6A/E (Sca-1) Alexa Fluor 700 (Clone: D7)	eBioscience	Cat#: 56-5981
Anti-Mouse Ly-6A/E (Sca-1) APC/Cy7 (Clone: D7)	Biolegend	Cat#: 108125
Anti-Mouse CD45 FITC (Clone: 30-F11)	eBioscience	Cat#: 11-0451
Anti-Mouse CD45 APC (Clone: 30-F11)	Biolegend	Cat#: 103111
Anti-Mouse CD45 PE (Clone: 30-F11)	Bioscience	Cat#: 12-0451
Anti-Mouse CD31 (PECAM-1) FITC (Clone: 390)	eBioscience	Cat#: 11-0311
Anti-Mouse CD31 (PECAM-1) APC (Clone: 390)	eBioscience	Cat#: 17-0311
Anti-Mouse CD31 (PECAM-1) PE-Cyanine7 (Clone: 390)	eBioscience	Cat#: 25-0311
Anti-Mouse CD140a (PDGF Receptor a) APC (Clone: APA5)	Biolegend	Cat#: 135907
Anti-Mouse CD140a (PDGF Receptor a) PE (Clone: APA5)	eBioscience	Cat#: 12-1401
Anti-Mouse CD24 APC-eFluor 780 (Clone: M1/69)	eBioscience	Cat#: 47-0242
Anti-Mouse CD24 PE (Clone: 30-F1)	eBioscience	Cat#: 12-0241
Anti-Mouse CD26 PerCP-Cyanine5.5 (Clone: H194-112)	eBioscience	Cat#: 45-0261
Anti-Mouse CD45.1 PE (Clone: A20)	eBioscience	Cat#: 12-0453
Anti-Mouse CD45.1 APC (Clone: A20)	eBioscience	Cat#: 17-0453
Anti-Mouse CD45.2 Alexa Fluor 700 (Clone: 104)	eBioscience	Cat#: 56-0454
Anti-Mouse CD11b PE (Clone: M1/70)	eBioscience	Cat#: 12-0112
Anti-Mouse Ly-6G (Gr-1) PE (Clone: RB6-8C5)	eBioscience	Cat#: 12-5931
Anti-Mouse CD19 APC-eFluor 780 (Clone: eBio1D3)	eBioscience	Cat#: 47-0193
Anti-Mouse CD3e APC-eFluor 780 (Clone: 145-2C11)	eBioscience	Cat#: 47-0031
Mouse Hematopoietic Lineage FITC Cocktail (Clone: 17A2, RA3-6B2, M1/70, TER-119, RB6-8C5)	eBioscience	Cat#: 22-7770
Anti-Mouse CD117 (c-Kit) APC (Clone: 2B8)	eBioscience	Cat#: 17-1171
Anti-Mouse CD34 Alexa Fluor 700 (Clone: RAM34)	eBioscience	Cat#: 56-0341
Anti-Mouse CD16/CD32 PE-Cyanine7 (Clone: 93)	eBioscience	Cat#: 25-0161
Rabbit anti-RFP (tdTomato)	Abcam	Cat#: ab62341
Goat anti-GFP	NovusBiologicals	Cat#: NB100-1770
Rat anti-CD45	NovusBiologicals	Cat#: NB100-77417
Goat anti-Perilipin	Abcam	Cat#: ab61682
Rabbit anti-Perilipin	Sigma	Cat#: P1873
Rat anti-CD31	Dianova	Cat#: DIA-310
Rat anti-Sca1	Abcam	Cat#: ab25195
Rat anti-BrdU	Cedarlane	Cat#: CL2700AP
Mouse anti-Aggrecan	Merck Millipore	Cat#: MABT84
Goat anti-Osteocalcin	BioRad	Cat#: 7060-1815
Goat anti-CD24	Abcam	Cat#: ab202963
Alexa Fluor 488 goat anti-rabbit	Abcam	Cat#: ab150077
Alexa Fluor 488 chicken anti-goat	Life Technologies	Cat#: A-21467
Alexa Fluor 488 donkey anti-rat	Life Technologies	Cat#: A-21208
Alexa Fluor 488 goat anti-mouse	Abcam	Cat#: ab150113
Alexa Fluor 568 goat anti-rabbit	Abcam	Cat#: ab175471
Alexa Fluor 594 donkey anti-rabbit	Life Technologies	Cat#: A-21207
Alexa Fluor 594 donkey anti-goat	Abcam	Cat#: ab150132
Alexa Fluor 680 donkey anti-rabbit	ThermoFisher	Cat#: A10043

(Continued on next page)

Continued

REAGENT or RESOURCE	SOURCE	IDENTIFIER
Anti-β-Actin Peroxidase-conjugated	Sigma	Cat#: A3854
Anti-human/mouse UCP1	R&D Systems	Cat#: MAB6158
Peroxidase goat anti-mouse	Abcam	Cat#: ab97023
Chemicals, Peptides, and Recombinant Proteins		
Calcein	eBioscience	Cat#: 65-0855-39
Propidium Iodide (PI)	Sigma	Cat#: P4170
Recombinant Mouse DPPIV/CD26 Protein	R&D Systems	Cat#: 954-SE
Diprotin A (Ile-Pro-Ile)	Sigma	Cat#: I9759
Sitagliptin	biomol	Cat#: Cay-13252-250
Cal-Rite Fixative	ThermoFisher	Cat#: 10599428
Roti-Histofix 4%	Carl Roth	Cat#: P087.3
Sudan Black B	Sigma	Cat#: 199664
Fluoromount-G	eBioscience	Cat#: 00-4958-02
Oil Red O	Sigma	Cat#: O0625
Alizarin Red S	Carl Roth	Cat#: A5533-25G
Alcian Blue 8GX	Sigma	Cat#: A3157
Crystal Violet	Sigma	Cat#: C0775
BrdU	Sigma	Cat#: B5002
D-Luciferin - K+ Salt Bioluminescent Substrate	Perkin Elmer	Cat#: 122796
MCDB201 Media	Sigma	Cat#: M6770
Dexamethasone	Sigma	Cat#: D-4902
L-Ascorbic acid 2-phosphate	Sigma	Cat#: A8960
Insulin-transferrin-selenium (ITS) mix	Sigma	Cat#: I3146
Linoleic acid-Albumin	Sigma	Cat#: L9530
Epidermal growth factor	PeproTech	Cat#: 315-09
Leukemia inhibitory factor	MerckMillipore	Cat#: ESG1107
Platelet-derived growth factor BB	PeproTech	Cat#: 315-18
Basic fibroblast growth factor	Sigma	Cat#: F0291
Indomethacin	Sigma	Cat#: I7378
Recombinant Human Insulin	Roche	Cat#: 11376497001
Isobutylmethylxanthine	Sigma	Cat#: I5879
3,3′,5-triiodo-L-thyronine (T3)	Sigma	Cat#: T6397
β-glycerophosphate	Sigma	Cat#: G9891
L-thyroxine	Sigma	Cat#: T0397
Transforming growth factor β1	PeproTech	Cat#: 100-21
Critical Commercial Assays		
DPP4 ELISA	ThermoFisher	Cat#: EMDPP4
RNeasy Plus Micro Kit	QIAGEN	Cat#: 74034
SMARTer PCR cDNA Synthesis kit	Clontech	Cat#: 634925
Advantage 2 PCR kit	Clontech	Cat#: 639207
Bioanalyzer DNA High-Sensitivity kit	Agilent Technologies	Cat#: 5067
Nextera XT DNA Sample Preparation Kit	Illumina	Cat#: FC-131
Nextera Index Kit	Illumina	Cat#: FC-131
Deposited Data		
RNA-seq Data	European Nucleotide Archive (ENA), http://www.ebi.ac.uk/ena	ENA: ERP013883
Experimental Models: Organisms/Strains		
Mouse: R6/2: C57BL/6J	The Jackson Laboratory	JAX: 000664
Mouse: R6/2: B6(Cg)-Tyr^c-2J/J	The Jackson Laboratory	JAX: 000058

REAGENT or RESOURCE	SOURCE	IDENTIFIER
Mouse: R6/2: B6.Cg-Tg(Gt(ROSA)26Sor-EGFP)I1Able/J	The Jackson Laboratory	JAX: 007897
Mouse: R6/2: B6.129S4-Pdgfra^{tm11(EGFP)Sor}/J	The Jackson Laboratory	JAX: 007669
Mouse: R6/2: B6;FVB-Tg(Zfp423-EGFP)7Brsp/J	The Jackson Laboratory	JAX: 019381
Mouse: R6/2: B6.SJL-*Ptprc^a Pepc^b*/BoyJ	The Jackson Laboratory	JAX: 002014
Mouse: R6/2: B6.129(Cg)-*Gt(ROSA)26Sor^{tm4(ACTB-tdTomato,-EGFP)Luo}*/J	The Jackson Laboratory	JAX: 007676
Mouse: R6/2: FVB.129S6(B6)-*Gt(ROSA)26Sor^{tm1(Luc)Kael}*/J	The Jackson Laboratory	JAX: 005125
Mouse: R6/2: B6.Cg-Tg(Prrx1-cre)1Cjt/J	The Jackson Laboratory	JAX: 005584
Mouse: R6/2: C57BL/6-Tg(Pdgfra-cre)1Clc/J	The Jackson Laboratory	JAX: 013148
Mouse: R6/2: B6;FVB-Tg(Adipoq-cre)1Evdr/J	The Jackson Laboratory	JAX: 010803
Mouse: R6/2: B6;129-Tg(Cdh5-cre)1Spe/J	The Jackson Laboratory	JAX: 017968
Mouse: R6/2: B6.Cg-Tg(Vav1-icre)A2Kio/J	The Jackson Laboratory	JAX: 008610
Mouse: R6/2: B6.Cg-Tg(Tek-cre)1Ywa/J	The Jackson Laboratory	JAX: 008863
Mouse: Dpp4^{tm1Nwa}	Marguet et al., 2000	MGI ID: 2150161
Sequence-Based Reagents		
qPCR Primer sets: please see Table S6	This paper	N/A

Note: In the table above, the superscript annotations should be rendered as: Pdgfra$^{tm11(EGFP)Sor}$, $Ptprc^{a}$ $Pepc^{b}$, $Gt(ROSA)26Sor^{tm4(ACTB-tdTomato,-EGFP)Luo}$, $Gt(ROSA)26Sor^{tm1(Luc)Kael}$, Dpp4^{tm1Nwa}.

CONTACT FOR REAGENT AND RESOURCE SHARING

Further information and requests for resources and reagents may be directed to and will be fulfilled by the Lead Contact, Tim J. Schulz (tim.schulz@dife.de). Animal strains used in this study are covered by MTAs prepared with the respective strain providers.

EXPERIMENTAL MODEL AND SUBJECT DETAILS

All procedures were approved by the ethics committee for animal welfare of the State Office of Environment, Health, and Consumer Protection (State of Brandenburg, Germany). Animals were housed in a controlled environment ($20 \pm 2°C$, 12/12 hr light/dark cycle), maintained on a SD (Ssniff, Soest, Germany), or fed a HFD (45% energy from fat, D12451, Research Diets, New Brunswick, NJ,USA) for 1 and 10 days. Male mice were used for all experiments at the indicated ages were applicable. All following mouse strains were obtained from The Jackson Laboratory: C57BL/6J, B6(Cg)-Tyr^{c-2J}/J (B6-albino), B6.Cg-Tg(Gt(ROSA)26Sor-EGFP)I1Able/J, B6.129S4-Pdgfra$^{tm11(EGFP)Sor}$/J (Pα-eGFP reporter), B6;FVB-Tg(Zfp423-EGFP)7Brsp/J (Zfp423-eGFP reporter), B6.SJL-*Ptprc^a Pepc^b*/BoyJ (CD45.1), B6.129(Cg)-*Gt(ROSA)26Sor^{tm4(ACTB-tdTomato,-EGFP)Luo}*/J (mTmG-reporter), FVB.129S6(B6)-*Gt(ROSA)26Sor^{tm1(Luc)Kael}*/J (Rosa26-Luciferase reporter), B6.Cg-Tg(Prrx1-cre)1Cjt/J, C57BL/6-Tg(Pdgfra-cre)1Clc/J, B6;FVB-Tg(Adipoq-cre)1Evdr/J, B6;129-Tg(Cdh5-cre)1Spe/J, B6.Cg-Tg(Vav1-icre)A2Kio/J, B6.Cg-Tg(Tek-cre)1Ywa/J. The strain Dpp4^{tm1Nwa} (Marguet et al., 2000; DPP4-KO) was provided from a colony maintained by Dr. Hua Fan from Charité University of Medicine, Berlin, Germany. Mouse strains expressing Cre-recombinase under promoter control of the hematopoietic (Vav1), endothelial (Cdh5 and Tek/Tie2), mesenchymal (Prx1 and PDGFRα), or mature adipocyte (AdipoQ) lineage markers were intercrossed with the mTmG-reporter mouse strain that constitutively expresses the membrane-bound red fluorescent protein tdTomato (from a loxP-flanked cDNA). Cre-mediated recombination leads to excision of the tdTomato-cassette and activates expression of green fluorescent protein instead. For transplantation experiments, Zfp423-eGFP reporter mice were either intercrossed with mTmG-reporter mice (rep^{tdTom}), or to AdipoQ-Cre mice and a lox-Stop-lox reporter strain expressing luciferase after Cre-mediated removal of the floxed Stop-cassette from the Rosa26-locus (rep^{AdiLuc}). Freshly sorted primary murine cells were used throughout this study and isolated by FACS and cultured as described before (Schulz et al., 2011; Steenhuis et al., 2008). Cells were therefore not authenticated. For cultivation, a complex medium of 60% DMEM low glucose (Invitrogen) and 40% MCDB201 (Sigma) was supplemented with 100 U/mL penicillin and 1,000 U/mL streptomycin (Invitrogen). 2% FBS, 1 × insulin-transferrin-selenium (ITS) mix, 1 × linoleic acid conjugated to BSA, 1 nM dexamethasone, and 0.1 mM L-ascorbic acid 2-phosphate (all from Sigma) were added. Before use, growth factors were added to the medium:10 ng/mL epidermal growth factor (PeproTech), 10 ng/mL leukemia inhibitory factor (MerckMillipore), 10 ng/mL platelet-derived growth factor BB (PeproTech), and 5 ng/mL basic fibroblast growth factor (bFGF; Sigma-Aldrich). The bFGF was added daily throughout the culture period except where stated otherwise. For adipogenic differentiation cells were induced for 48 hr after three days of expansion, followed by a differentiation period of 5 days. For adipogenic differentiation, induction medium (growth medium without growth factors) containing 5 μg/mL human insulin (Roche Applied Science), 50 μM indomethacin, 1 μM dexamethasone, 0.5 μM isobutylmethylxanthine, 1 nM 3,3′,5-triiodo-L-thyronine (T3) (all from Sigma-Aldrich) was added for 48 hr, followed by further differentiation in growth medium without growth factors and the addition of T3 and insulin only. Oil Red O staining was performed by fixing cells with 4% Histofix for 15 min at room temperature. For the preparation of Oil Red O working solution, a 0.5% stock solution in isopropanol was diluted with distilled water at a ratio of 3:2. The working solution was filtered and applied to fixed cells for at least one hour at room temperature. Cells were washed four times with tap

water before evaluation. For quantification, Oil Red O was extracted by adding a defined volume of isopropanol and absorbance was read in a micro-plate reader (Synergy H1, BioTek) at 510 nm. To induce osteogenic differentiation, pre-confluent cells were supplemented with osteogenic medium (DMEM low glucose (Invitrogen)) with 10% FBS, 100 nM Dexamethasone, 0.2 mM L-ascorbic acid 2-phosphate, 10mM β-glycerophosphate, and 50 ng/mL L-thyroxine) for 14 days. Cells were then formalin-fixed and stained with 2% Alizarin Red S (Roth) in distilled water. Wells were washed twice with PBS and once with distilled water. De-staining was conducted to quantitatively determine mineralization by adding a 10% cetylpyridinium chloride solution. Absorbance was measured in a micro-plate reader (Synergy H1, BioTek) at 570 nm. A micromass culture was used for the chondrogenesis assay. To this end, a 5 μL droplet of cell suspension (appr. 1.5×10^7 cells/mL) was pipetted in the center of a well (48-well plate). After cultivating the micromass culture for 2 hr in the incubator, warm chondrogenic media (DMEMhigh (Invitrogen)) with 10% FBS, 100 nM Dexamethasone, 1 μM L-ascorbic acid-2-phosphate, 10x ITS mix, and 10 ng/ml Transforming growth factor β1) was added. Cell media was changed every other day. After 21 days cells were fixed and stained with 1% Alcian-Blue staining (Sigma) for 30 min at room temperature. Cells were rinsed three times with 0.1 M HCl. To neutralize acidity a washing step with dH2O was conducted before microscopic analysis. For DPP4 in vitro experiments cell populations were differentiated with adipogenic or osteogenic assays as described above. Mouse recombinant DPP4 (250 ng/mL; R&D Systems) or DPP-4 inhibitor Sitagliptin (100 μM; biomol) were added to differentiation cocktails from day 3 (adipogenic induction) during adipogenesis or day 0 during osteogenesis until the end of differentiation experiments. DPP4 secretion into cell culture media was determined by ELISA (ThermoFisher). Either supernatant of freshly isolated tibia explants maintained in culture media for 24 hr or supernatant from cell populations following 10 days of adipogenic differentiation were used. CFU-F assay was conducted as follows: Freshly isolated cell populations were seeded in expansion media at 500 cells per 6-well plate. Medium was changed every other day. At day 10 cells were fixed and stained with Crystal Violet (Sigma). Colonies consisting of more than 20 cells were counted as CFU. At least 6 independent assays were performed per cell population. For total recovery rate experiments cell populations were seeded as described for the CFU-F assay. Analysis of fixed and Crystal Violet stained cell populations was conducted on day 7, 11, and 15 by quantification of total cell invasion area of well-plate surface using ImageJ software.

METHOD DETAILS

Flow cytometry & cell sorting
Flow cytometry and cell sorting were performed on a FACS Aria III cell sorter (BD Biosciences) and analyzed using FlowJo software (Tree Star). Soft-tissue free bones (tibia/femur) were crushed with bone scissors and incubated for 1 hr in a shaking water bath at 37°C in 10 mL of 20% FBS/PBS containing 0.5% type-2 collagenase (CellSystems). The suspension was filtered through a 70 μm mesh to remove bone fragments and centrifuged at 1200 rpm for 5 min at 4°C. The pellet was re-suspended in ACK (Ammonium-Chloride-Potassium) lysing buffer to eliminate red blood cells and centrifuged again at 1200 rpm for 5 min at 4°C. The pellet was re-suspended in 100 μL sorting buffer (2% FBS/PBS) and stained with antibodies for at least 30 min at 4°C. The applied FACS antibodies can be found in the Key Resources Table. Living cells were gated for lack of PI (propidium iodide; 1:1,000 diluted stock solution: 1 μg/mL in water) fluorescence and accumulation of Calcein (1:1,000 dilution; stock of 1 mg in 215 μL DMSO). Compensation, fluorescence-minus-one control based gating, and FACS-isolation was conducted as described before using the antibody combinations as indicated in the respective figures and legends (Schulz et al., 2011).

Single-cell clonal assays
For the co-culture approach, a feeder layer of CD45⁻CD31⁻Pα⁺ cells was isolated from long bones of 8-weeks old male C57BL/6J mice and seeded in 100 μL of expansion medium at 750 cells per well of a 96-well plate. On the next day, a single CD45⁻CD31⁻Sca1⁺CD24⁺ tdTomato⁺ cell freshly isolated from 8-weeks old male Rosa26-mTmG mice was FAC-sorted into each well. Cells were expanded for 10 days to sub-confluency with media changes every other day. After 10 days, clonal expansion of a single cell was verified by fluorescence microscopy. Wells containing a readily detectable single colony of tdTomato⁺ cells were trypsinized, washed, and collected in 100 μL sorting medium. Five to ten cells (per condition) of each clone were directly FAC-sorted onto freshly prepared 96-well plate feeder layers of expanded CD45⁻CD31⁻Pα⁺ cells for adipogenic and osteogenic differentiation protocols, or onto a micromass culture for chondrogenic differentiation. At the end of the differentiation assays clones were analyzed for their differentiation capacity by immunocytochemistry. A tdTomato positive clone was considered adipogenic if it co-stained with Perilipin, osteogenic if it co-stained with Osteocalcin, and chondrogenic if it co-stained with Aggrecan. Alternatively, in a feeder cell-free assay, a single CD45⁻CD31⁻Sca1⁺ CD24⁺ cell, freshly isolated from 8-weeks old male C57BL/6J mice, was FAC-sorted into a well of a 96-well plate without feeder cells. Single cells were expanded for 10 days with media changes every other day. After 10 days, clones giving rise to colonies were re-seeded in a new 96-well plate and expanded until sub-confluency. Clones were then used for tri-differentiation assays. At the end of differentiation Oil Red O staining was conducted for adipogenesis and immunocytochemistry for osteogenesis (Osteocalcin) and chondrogenesis (Aggrecan). Images were acquired with a Keyence BZ-9000 (Biorevo) fluorescence microscope.

Histology
Isolated bones were cleaned from surrounding tissue and fixed/decalcified in Richard-Allan Scientific Cal-Rite fixative (Thermo Scientific), followed by paraffin embedding. Sections (3 μm) were used for immunohistological staining or H&E overview staining. For immunohistochemistry sections were de-paraffinized and re-hydrated in xylene and decreasing ethanol concentrations. Heat-mediated antigen retrieval was conducted by placing sections in blocking buffer (40 mM Tris and 1.2 mM EDTA in distilled water) in a

microwave for 5 min at 330 W. Slides were left for cooling and rinsed with water. Nearly dried samples were circled with a PAP pen (Kisker) and incubated with blocking solution (1% BSA/PBS) for 60 min at room temperature. Primary antibodies, diluted in 1% BSA/PBS, were added and samples were incubated in a humidified chamber at 4°C overnight. Sections were washed with PBS three times. Secondary antibody and DAPI nucleus staining were applied for 10 min at room temperature in the dark. Samples were washed twice with PBS. To reduce auto-fluorescence 0.3% Sudan Black solution (in 70% EtOH) was applied for 20 min. Sections were washed three times and mounted with Fluoromount G (eBioscience, GER). Samples were stored at 4°C in the dark before evaluation via fluorescence microscopy. For the quantification of the different bone-resident populations, bone marrow regions of 0.05 mm^2 from bone sections were selected on fluorescence images. For immunocytochemistry, fixated cells in well plates were permeabilized with 0.1% Triton X-100 solution and blocked with 3% BSA in PBS. Antibodies were used as listed in the Key Resources Table. For nuclear staining specimen were treated with DAPI. Sections and cells were analyzed using a Keyence BZ-9000 (Biorevo) fluorescence microscope (for up to two fluorescences) or a Zeiss confocal laser scanning microscope (LSM) 700 (for three fluorescences).

Sternal transplantation

Sorted cell populations (see Figure S2L) from luciferase-expressing rep^{AdiLuc} or tdTomato-expressing rep^{tdTom} mice were subcutaneously injected at 1.5×10^4 cells in a 50% matrigel suspension into the sternal area of B6-albino mice. Eight weeks after transplantation, engrafted tissues were excised, fixed, and histologically analyzed. Mice injected with cells from rep^{Luc} animals were additionally subjected to Luciferase imaging with an IVIS imaging system (Perkin Elmer) before sacrifice. To this end, animals were intraperitoneally injected with luciferin (150 mg/kg) and subsequently anesthetized. After 12 to 18 min, the animals were imaged. Image analysis was performed with Living Image 4.4 software (Xenogen).

BrdU cell proliferation in vivo assay

For 24 hr experiments mice were i.p.-injected with a single dose of 100 mg BrdU/kg (Sigma Aldrich) diluted in sterile PBS. Mice receiving a SD or HFD for ten days were given BrdU via drinking water at a concentration of 0.5 mg/mL. Drinking water was refreshed every other day. For single-cell immunostaining approximately 2×10^3 cells/mouse of each population of interest were double-sorted on glass coverslips pre-coated with a 5 μL drop of DMEM(low). Coverslips were incubated for 30 min, allowing cells to attach. Cells were fixed by gently adding 4% Histofix for 10 min and washed three times for 3 min with PBS. Permeabilization solution (0.2% saponin/PBS) was applied for 6 min. Washing solution (0.02% saponin/PBS) for 5 min was followed by administering DNA-denaturation solution (2 M HCl in 0.02% saponin/PBS) for 20 min at 37°C. Cells were washed for 5 min and blocked for 30 min with 2% BSA in washing solution. Incubation with anti-BrdU antibody (Cedarlane) in blocking solution was done overnight at 4°C. On the next day, three times washing for 10 min and incubation with Alexa Fluor 488 donkey anti-rat (FisherScientific) and DAPI staining in blocking solution for 30 min at room temperature in the dark was performed. Cells were washed with washing solution three times and PBS once. Coverslips were mounted with Fluoromount G (eBioscience). Samples were stored at 4°C in the dark before evaluation via fluorescence microscopy (Keyence). The percentage of BrdU-positive cells within each population was calculated as compared to total numbers of DAPI-positive cells.

Competitive hematopoietic reconstitution assay

Animals were given antibiotics via drinking water and an analgetic one week and two days, repectively, before experiments. C57BL/6J recipient mice were lethally irradiated with a single dose of 7.5 Gy. For reconstitution assays, 150 LT-LSK cells from donor mice expressing the CD45.1 allele were mixed with 1×10^5 freshly isolated whole bone marrow supporting cells (collected by flushing the BM from long bones) from C57BL/6J mice (CD45.2) in addition to 1.5×10^4 cells of one of the investigated populations isolated from rep^{dtom} mice, then injected in the medullary cavity of the tibia through the proximal articular surface. For the investigation of acute effects peripheral blood, tibia bone marrow, and tibia bones were analyzed by flow cytometry five weeks post irradiation. For long-term experiments blood was taken every four weeks and tibia bone marrow and tibia bones were analyzed 16 weeks post irradiation. Red blood cells were lysed, followed by antibody staining to distinguish between different blood cell populations (as listed in the Key Resources Table). For evaluation of donor chimerism the frequency of donor fraction (CD45.1$^+$:CD45.2$^-$) was calculated.

Fracture model

Mice were given an analgetic (MediGel, ClearH$_2$O) starting two days prior to surgery. Anesthetized mice were injected with 1.5×10^4 cells in a 50% matrigel suspension through the proximal articular surface of the tibia. A steel pin (diameter 0.35 mm) was inserted into the medullary cavity for stabilization and a fracture was induced with scissors 0.5 cm distal from the knee. At the indicated time point after fracture induction, tibiae were harvested for analyses. After removal of the pin from extracted tibiae, μCT analysis was conducted with LaTheta LCT-200 (Hitachi-Aloka) using manufacturer's pre-defined parameters for isolated bone measurements. Alternatively, tibiae were fixed and decalcified followed by paraffin embedding and sectioning at 3 μm per slice. Samples were stained using SafraninO/Fast green and Movat Pentachrome. ImageJ software was used for computer-assisted histomorphometric analysis of fracture calluses. Six representative sections of each callus were analyzed for bone, fibrous, and cartilaginous tissue areas in a blinded manner. For DPP4 in vivo experiments mice received a daily dose of PBS, Diprotin A (5 mg/kg body weight; Sigma) or Sitagliptin (10 mg/kg body weight; biomol) i.p. for 9 consecutive days. For fracture healing experiments application started two days before induction of injury/cell injection. Fracture healing was assessed one day after the last DPP4-inhibitor administration.

Capture, Library Preparation, and Sequencing of cell population

A total of 17,000 CD45$^-$CD31$^-$Sca1$^-$Zfp423$^+$, 50,000 CD45$^-$CD31$^-$Sca1$^+$CD24$^-$, 5,000 CD45$^-$CD31$^-$Sca1$^+$CD24$^+$ and 30,000 CD45$^-$CD31$^-$Sca1$^-$Pα^+ cells were FAC-sorted from bones of 4 mice (the 3 biological replicates were done on 3 different days), collected in a 1.5 mL Eppendorf tube containing 50 μL RLT Plus Buffer (QIAGEN) supplemented with 1% 2-Mercaptoethanol, immediately frozen in dry-ice and kept at -80°C. The time elapsed between mouse euthanasia and the termination of the FACS procedure was $\sim$400 min. RNA extraction, reverse transcription and cDNA pre-amplification, Nextera XT libraries and sequencing of the cell populations was done as previously described and according to the manufacturer's instructions. Briefly, RNA was extracted using the RNeasy Plus Micro Kit (QIAGEN), together with genomic DNA eliminator (QIAGEN). Reverse transcription and cDNA pre-amplification were performed using the SMARTer PCR cDNA Synthesis kit (Clontech) and the Advantage 2 PCR kit (Clontech). cDNA was harvested and quantified with the Bioanalyzer DNA High-Sensitivity kit (Agilent Technologies). Libraries were prepared using the Nextera XT DNA Sample Preparation Kit and the Nextera Index Kit (Illumina). Multiplexed libraries were pooled, and paired-end 100-bp sequencing was performed on one flow–cell (two lanes) of an Illumina HiSeq 2500.

RNA-seq data processing and analysis

Sequencing data were aligned to the *Mus musculus* genome (Ensembl version 38.82) using GSNAP (version 2014-10-07) with default parameters. HTseq-count was used to count the number of reads mapped to each gene (default options). Almost all libraries showed good quality, with sizes ranging between 2-3.5x10^7 read counts and a fraction of reads mapped to exons greater than 75% (Figure S7). One library yielded less than 300 reads and was excluded from downstream analysis. The data was normalized for sequencing depth using size factors. The union of the top 1,000 genes expressed in each library was selected, which resulted in a list of 2,120 genes. Principal component analysis was carried out on the standardized log10-transformed normalized counts (after adding a pseudo-count of 1 to avoid infinities). Hierarchical clustering analysis was performed using Euclidean distances with Ward's method on the same dataset. Differentially expressed genes between groups of libraries were identified by using the bioconductor R-package DESeq2 library at a FDR of 0.1. Genes that were not detected in any library were removed prior to the analysis and possibly confounding factors were taken into account (i.e., the animal each sample was taken from). RNA-seq data was statistically analyzed using the R-statistical package and Paleontological Statistics (PAST, version 3.10, http://folk.uio.no/ohammer/past/, accessed December 2015). For DE analyses, gene expression was compared between all investigated cell populations. A p-value of < 0.05 was used as a cut-off for differentially expressed genes. Heat-maps contain representative top-regulated genes, which were further divided by known cell type specific functions as previously described in the literature and unknown novel marker genes.

Gene expression analysis

Total RNA isolation and gene expression analysis was conducted using standard methods as described before (Schulz et al., 2011) using column-based RNA-isolation, reverse transcription for cDNA synthesis, and SYBR green-based detection during quantified real-time PCR. Primer sequences were used as noted in the Key Resources Table.

QUANTIFICATION AND STATISTICAL ANALYSES

All data are presented as mean ± standard error of the mean (SEM). The sample size for each experiment and the replicate number of experiments are included in the figure legends. Statistical significance was defined as p < 0.05. Statistical analyses were performed using unpaired, two-tailed Student's t test or Mann-Whitney-U-test where applicable for comparison between two groups, and an ANOVA test was used for experiments involving more than two groups (GraphPad Prism; version 6.04).

DATA AND SOFTWARE AVAILABILITY

Data Resources

The accession number for the gene expression data generated by RNA-seq data reported in this study is ENA: ERP013883 (http://www.ebi.ac.uk/ena).